

# On the Spatial Distribution of Luminous Blue Variables, B[e] Supergiants, and Wolf-Rayet stars in the Large Magellanic Cloud

JOHN C. MARTIN <sup>1</sup>, ROBERTA M. HUMPHREYS <sup>2</sup>, AND KRIS DAVIDSON <sup>2</sup>

<sup>1</sup>*University of Illinois Springfield*

<sup>2</sup>*Minnesota Institute for Astrophysics, University of Minnesota*

## ABSTRACT

We examine the spatial distributions of LBV's, B[e] supergiants, and W-R stars in the LMC, to clarify their relative ages, evolutionary states, and relationships. This survey employs a reference catalog that was not available for previous work, comprising more than 3900 of the LMC's most luminous stars. Our analysis shows that LBV's, B[e] supergiants, and WR's have spatial distributions like normal stars with the same spectral types and luminosities. Most LBV's are not isolated, nor do they require binary or multiple status to explain their spatial relationship to other populations. There are two likely exceptions: one lower-luminosity LBV and one LBV candidate are relatively isolated and may have velocities that require additional acceleration. The B[e] supergiants are spatially and kinematically more dispersed than LBV's, suggesting that they belong to an older population. The most luminous early-type WN's are most closely associated with the evolved late O-type supergiants. The high luminosity late WN's, however, are highly concentrated in the 30 Dor region which biases the analysis. The less luminous WN's and WC's are associated with a mix of evolved late B, A-type, and yellow supergiants which may be in a post-red-supergiant phase. Spatial distributions of the less luminous WN, WC, and WN3/O3 stars reinforce proposed evolutionary links among those subtypes. Our analysis also demonstrates the importance of using a comprehensive census, with reference populations clearly defined by spectral type and luminosity, and how small number statistics, especially combined with spatial clustering, can invalidate some commonly-cited statistical tests.

*Keywords:* Massive stars(732), Large Magellanic Cloud(903), Luminous blue variable stars, B[e] supergiant stars, Wolf-Rayet stars

## 1. INTRODUCTION

The important final stages in the evolution of massive stars, whether they end as supernovae or collapse directly to black holes, remain uncertain. The majority of massive stars ( $9 - 40 M_{\odot}$ ) will pass through the red supergiant stage. For most, this is their terminal phase. However, those with

initial mass greater than about  $40 M_{\odot}$ , above the empirical upper luminosity boundary, do not evolve to the red supergiant stage (Humphreys & Davidson 1979, 1994). Many terminal explosions exhibit interaction with circumstellar material from prior mass loss, even high mass loss events. But understanding the association of the probable SNe progenitors with the classes or groups of luminous evolved stars known for high mass loss is complicated by the latter’s relative scarcity and their different evolutionary histories. They include the Luminous Blue Variables (LBVs), B[e] supergiants (B[e]sg), Wolf-Rayet stars (WR), the yellow and red hypergiants, and the rare giant eruptions.

Various authors have argued about the evolutionary state of LBVs or S Dor variables and their relationship to other evolved massive stars, including the origin of their underlying instability. Smith & Tombleson (2015) suggested that LBVs are physically isolated from the population of young O-type stars in the Magellanic Clouds, and concluded that they are runaway stars that have gained mass in binary systems and have been accelerated. Humphreys et al. (2016) and Davidson et al. (2016) tested their assumptions and showed that the confirmed LBVs are associated with evolved massive stars. The Smith and Tombleson sample was a mixed population. When the non-LBVs were removed, the classical LBVs were associated with later O-type stars, while the less luminous LBVs were associated with more evolved supergiants. Aadland et al. (2018) recognized the incompleteness of the O and B star reference populations in the LMC and used a photometrically selected sample of bright blue stars. They similarly concluded that LBVs are not more dispersed from massive stars but are spatially distributed like the WR stars.

These studies affirm the need for a more comprehensive reference sample of spectroscopically selected luminous stars for comparison, which can be separated by spectral type and luminosity. In our own galaxy, dust and gas in the Galactic plane obscure most of the massive star population from view and even with the advances from Gaia, distances to stars in the Milky Way may be uncertain. In Local Group galaxies like the LMC, SMC, M31 and M33, the stars are essentially at the same distance. These star forming galaxies with large numbers of young, massive stars, present a more complete picture of the population of the upper HR Diagram.

Fortunately, the LMC is well-studied in this respect with many spectroscopic and photometric surveys which when combined yield a formidable sample for analyzing the spatial distribution of evolved luminous stars. Previous studies mostly excluded the 30 Doradus region due to extreme crowding and uncertain extinction. In Martin & Humphreys (2023) we presented a spectroscopically-selected HR-Diagram for the most luminous stars in the LMC combining data from many surveys including the VFTS survey of 30 Doradus (Evans et al. 2011) plus the evolved A-type supergiants, and the yellow (YSGs) and red supergiants (RSGs).

Several additional early O-type and later type stars from the VFTS survey have since been added to the lists in our 2023 paper. They are included in Appendix A. The HR-Diagram with these new stars is shown in Figure 1.

We use this catalog of 3910 luminous stars of all spectral types to investigate the spatial distributions of the LBVs, B[e]sg and WR stars. In the following sections, we describe our selection of the samples, their spatial distributions, and our nearest-neighbor analysis. We summarize our results based on their spatial distributions and their kinematics in §4 and highlight our conclusions in the last section.

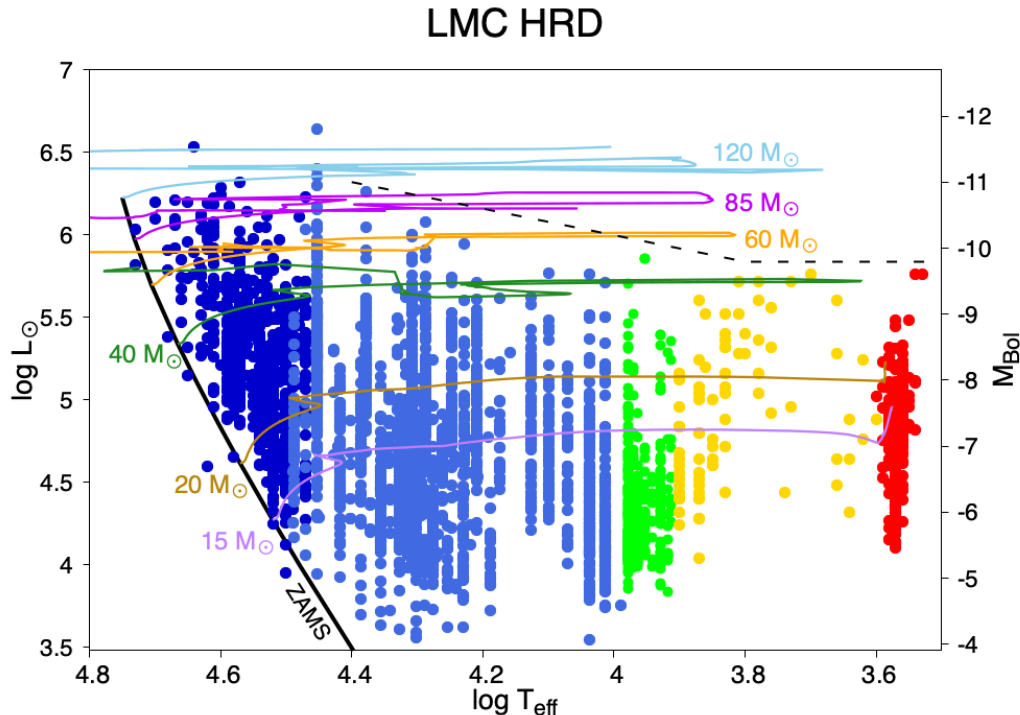


**Figure 1.** The Hertzsprung-Russell diagram for the most luminous and massive stars in the Large Magellanic Cloud. The Zero Age Main Sequence (ZAMS) is noted with a solid black line. The Humphreys/Davidson limit (Humphreys & Davidson 1979, 1994) is noted with the dashed black line. Stars are color coded: O-type = dark blue, B-type = light blue, A-type = green, YSG = yellow, RSG = red. The ZAMS and evolutionary tracks are adopted from Eggenberger et al. (2021)  $Z = 0.006$  non-rotating models (LMC is  $Z = 0.006$ ).

## 2. LBVS, B[E]SG, AND WOLF-RAYET STARS IN THE LMC

### 2.1. *LBVs*

LBVs are a relatively small group of evolved massive stars recognized by their characteristic S Dor spectroscopic and photometric variability. In its enhanced mass loss phase, i.e the LBV eruption or maximum-light phase, the star increases in visual brightness by 1 to 2 magnitudes. Its spectrum changes from its hot, quiescent state to a cooler type resembling a late A to F-type supergiant ( $T_{eff} \sim 7000 - 8500$  K) due to its expanded photosphere or optically thick wind. See the HR-Diagrams in Humphreys & Davidson (1994) and Humphreys et al. (2016) for examples of their apparent transits at nearly constant luminosity. The star may stay in this state of enhanced mass loss for several years. During their quiescent state, LBVs lie along what is known as the LBV or S Dor instability strip (Wolf et al. 1981; Humphreys & Davidson 1994).

It is important to avoid confusing LBV/S Dor variability with giant eruptions which significantly increase their bolometric luminosities, with higher mass loss, and shorter duration at maximum light. The latter are sometimes referred to as supernova imposters. See the recent review by Davidson (2020) for a more complete discussion.

Humphreys & Davidson (1994) divided the LBVs into two groups based on their luminosities in quiescence; the classical LBVs with luminosities above the Humphreys-Davidson limit and the less luminous LBVs. These two groups have different evolutionary histories. The more luminous classical

LBVs do not become red supergiants (RSGs) while the less luminous group can evolve to the RSG stage and may be in a post-RSG state. Table 1 includes three classical LBVs and five in the less luminous group, plus five candidates. The candidates are those that share some characteristics with LBVs but without an observed S Dor eruption. Figure 2 shows the confirmed LBVs on a schematic HR Diagram.

Due to the infrequency of the S Dor variability, very few evolved hot stars have been confirmed as LBV/S Dor variables. The confirmed LBVs in Table 1 are the same stars that were in [Humphreys et al. \(2016\)](#) with two additional members, HDE 269582 and HD 269216 from [Walborn et al. \(2017\)](#). HD 269582 was listed in [Humphreys et al. \(2016\)](#) as a candidate LBV. The entire class of candidate LBVs should be approached with caution, because there is no good way to estimate what fraction of them are true LBVs.

**Table 1.** Luminous Blue Variables

RAJ2000	DecJ2000	Name	Sp. Type	$M_{Bol}$	References <sup>a</sup>
Classic LBVs					
79.55979	-69.25028	S Dor (HD 35343)	B1	-9.8	1,2,11
81.96943	-68.98569	HDE 269582 (Sk -69 142a) <sup>b</sup>	Ofpe/WN10h	-9.7	9,11
84.18208	-69.49650	R127 (HDE 269858)	Ofpe/WN9	-10.5	1,3,11
Less-Luminous LBVs					
75.53073	-71.33703	R71 (HDE 269006)	B5:I	-9.2	5,6,11
78.37821	-69.53989	HDE 269216 (Sk -69 75)	B7:Iae	-9.1	11
79.48363	-69.26869	R85 (HDE 269321)	B5Iae	-8.5	8
82.71446	-69.04963	R110 (HDE 269662)	B6 I	-8.9	7
84.71508	-69.13531	R143	B9 - A	-8.6	4,11,13
Candidate LBV					
82.85635	-69.09404	S119 (HDE 269687)	WN11h	-9.8	9
82.96783	-68.54413	R116 <sup>c</sup> (HDE 269700)	B1.5aeq	-10.6	4, 14
83.92683	-69.67734	HD 37836	B0e(q)	-11.4	15
84.99476	-69.734465	R149 (Sk -69 257)	O8.5 II((f)))	-9.7	12
85.43607	-69.58747	Sk -69 279	O9f	-9.7	10
86.46641	-67.24054	S61 (Sk -67 266)	WN11h	-9.7	9

<sup>a</sup>(1) [Stahl & Wolf \(1986\)](#), (2) [Leitherer et al. \(1985\)](#), (3) [Stahl et al. \(1983\)](#), (4) [Feast et al. \(1960\)](#), (5) [Wolf et al. \(1981\)](#), (6) [Mehner et al. \(2013a\)](#), (7) [Stahl et al. \(1990\)](#), (8) [Massey et al. \(2000\)](#), (9) [Crowther & Smith \(1997\)](#), (10) [Conti et al. \(1986\)](#), (11) [Walborn et al. \(2017\)](#), (12) [Fariña et al. \(2009\)](#), (13) [Agliozzo et al. \(2019\)](#), (14) [Ardeberg et al. \(1972\)](#), (15) [Shore & Sanduleak \(1984\)](#)

<sup>b</sup>Included as a candidate LBV in [Humphreys et al 2016](#). It is assigned a luminosity both higher ([Crowther & Smith 1997](#)) and lower ([Crowther et al. 2023](#)) than the Humphreys-Davidson Limit ( $M_{bol} < -9.7$ ) with the discrepancy likely due to a difference in adopted extinction. We have included it here as a classic high luminosity LBV because [Walborn et al. \(2017\)](#) noted strong spectroscopic similarities with LBV R127, and argued it is a similar case.

<sup>c</sup>[Agliozzo et al. \(2021\)](#) included R116 as a confirmed LBV. [van Genderen \(2001\)](#) listed it as an LBV based on 19th century eye estimates that R116 was about half a magnitude brighter than modern photometry from different sources since 1956 ([van Genderen & Sterken 1999](#)). It has not shown any S Dor variability or any significant variability in 70 years. We include it as a candidate LBV.



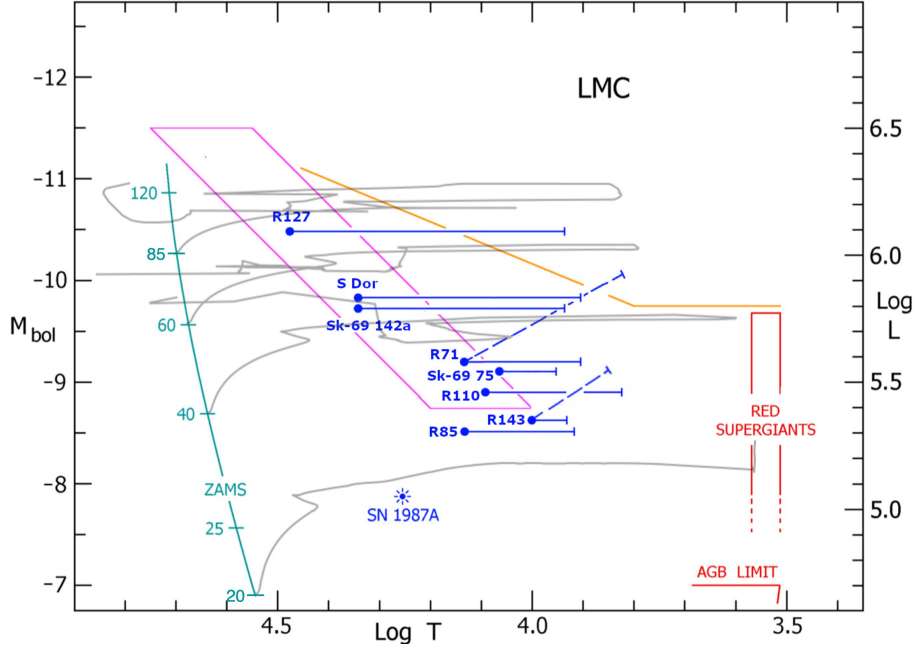


**Figure 2.** A schematic HR diagram of the LBVs in the LMC discussed in the text. The apparent transits of the LBV during outburst are shown as straight blue lines. The LBV/S Dor instability strip is outlined in pink, and the empirical upper luminosity boundary is shown in orange. Evolutionary tracks from Eggenberger et al. (2021) are shown in gray for  $20 M_{\odot}$ ,  $40 M_{\odot}$ ,  $60 M_{\odot}$ , and  $85 M_{\odot}$ .

R143 has a checkered history. It is noted here because it is pertinent to discussion in later sections. It was formerly considered a classical LBV, but its identification in quiescence with HDE 269929, a late O-type star, by Parker et al. (1993) was due to a misidentification (AglioZZo et al. 2019). However, the most recent spectroscopic observations summarized by Walborn et al. (2017) show variation between late B and A-type. Based on its earlier F-type spectrum, observed from 1952 to 1985 (Feast et al. 1960; Melnick 1985), R143’s maximum light or LBV eruption lasted more than 30 yrs. AglioZZo et al. (2019) report a temperature of 8500 K and  $M_{Bol}$  of -8.6 mag in its current quiescent state. Thus during its high mass loss F-type supergiant phase, R143’s bolometric luminosity, -9.4 to -9.1 mag, may have increased compared to its luminosity in quiescence. In that respect, it may be like R71 which is currently experiencing an apparent increase in luminosity during its LBV eruption (Mehner et al. 2013b; Walborn et al. 2017). R143 is included in Table 1 as a less luminous LBV.

In quiescence or their normal hot star state LBVs are often late-WN type stars or are classified as mid to late B-type supergiants with emission lines. Consequently, many hot, emission line stars may be confused with LBVs. The most common are the B[e]sgs which spectroscopically resemble LBVs. One of the distinguishing characteristics of B[e]sgs is the presence of warm dust in the near-infrared not observed in LBVs (Kraus 2019; Lamers et al. 1998). The B[e] supergiants are included here in Table 2.

Several published lists of LBVs and candidates include numerous B[e]sgs. For example, Richardson & Mehner (2018) included six B[e]sg in the LMC plus  $\alpha$  Cyg variables R74, R78, and HD 269604 (van Genderen & Sterken 1999). Aadland et al. (2018) listed three known B[e]sg and two  $\alpha$  Cyg variables. AglioZZo et al. (2021) separated the B[e]sg, but included two non-LBVs, R81 and R99, and

**Table 2.** B[e] Supergiants

RAJ2000	DecJ2000	Name	Sp. Type	$M_{Bol}$	Status <sup>a</sup>	References <sup>b</sup>
Early						
74.40317	-67.79371	LHA 120-S 12	B0.5Ie	-8.7	Confirmed	1
78.47073	-67.44856	HD 34664	B0/0.5I[e]	-10	Established	2
81.82433	-66.36823	LHA 120-S 35	Hot	-8.2	Established	3
82.09463	-69.14219	HDE 269599	B1	-10.4	Established	5
84.10776	-69.38218	HD 37974	B0.5e	-10.5	Established	5
85.05554	-69.37958	HD 38489	B0	-9.8	Established	6
85.43232	-69.62732	LHA 120-S 137	B1aePCyg	-5.8	Established	7
86.37289	-68.19608	LHA 120-S 59	B0.5IIIe	-5.2	Established	4
Mid						
78.41205	-69.35230	HDE 269217	B5/6Ia[e]	-8.8	Established	10
Late						
73.68104	-70.35762	ARDB 54	A0-II	-6.1	Confirmed	12
74.19606	-69.84095	HDE 268835	B8[e]	-8.9	Established	1
79.13247	-68.36926	LHA 120-S 93	A0:I	-6.7	Established	11

<sup>a</sup>Classification status as assigned by [Kraus \(2019\)](#)

<sup>b</sup>(1) [Zickgraf et al. \(1986\)](#), (2) [Oey \(1996\)](#), (3) [Gummersbach et al. \(1995\)](#), (4) [Reid & Parker \(2012\)](#), (5) [Shore & Sanduleak \(1984\)](#), (6) [Shore & Sanduleak \(1983\)](#), (7) [Fariña et al. \(2009\)](#), (8) [Ardeberg et al. \(1972\)](#), (9) [Rousseau et al. \(1978\)](#), (10) [Cidale et al. \(2001\)](#), (11) [Sanduleak \(1970\)](#), (12) [Condori et al. \(2019\)](#)

two  $\alpha$  Cyg variables as candidates. The kinematic study by [Aghakhanloo et al. \(2022\)](#) also listed five non-LBV stars and a B[e]sg. The non-LBVs in [Aghakhanloo et al. \(2022\)](#) were previously discussed in [Humphreys et al. \(2016\)](#). They are; R84 a composite B0 Ia + M4 Ia, Sk -69° 271 classified B4I/III, and R99, a peculiar Ofpe/WN9 star but not considered an LBV. The description of these stars is not repeated here. R81 and MWC 112, however, require some discussion.

*R81* ( $=$  *HDE 269128* = *Hen S86*) is not an LBV or candidate. It is a known eclipsing binary ([Stahl et al. 1987](#); [Tubbesing et al. 2002](#)). R81's spectroscopic and photometric variability are due to its orbital motion. The primary is an early B-type supergiant, but the secondary is not observed and assumed to be a small, cooler star. The pair is an interacting binary with a short orbital period, and [Tubbesing et al. \(2002\)](#) hypothesize that the secondary may be surrounded by material accreted from the primary. They find that the spectroscopic variations are synchronized with the orbit. [Aghakhanloo et al. \(2022\)](#) refer to the LBV, presumably the hot primary, but no S Dor variability has been reported. [Aglozzio et al. \(2021\)](#) also list it as a candidate LBV.

[Humphreys et al. \(2016\)](#) described *MWC 112* as an F5 Ia supergiant and identified it with Sk -69° 147 based on its entry in SIMBAD. A closer examination by [Humphreys et al. \(2023\)](#) showed that Sk -69° 147 is indeed a normal F-type supergiant. However, MWC 112 is *HDE 268582* = Sk -69° 142a ([van Genderen & Sterken 1996](#)), now recognized as an LBV (Table 1). [Aghakhanloo et al. \(2022\)](#) list MWC 112 and Sk -69° 142a separately in their Table 1. It is unclear which star they observed as MWC 112. The entry in SIMBAD has been corrected.

## 2.2. B[e] Supergiants

The evolutionary state of the B[e]sg is uncertain. Like the LBVs, they are massive post-main sequence stars. Some authors have argued for a post-RSG or post-yellow/warm supergiant stage (Kastner et al. 2010; Aret et al. 2012) and others for a pre-RSG state (Oksala et al. 2013; de Wit et al. 2014). In addition to their emission line spectra, the B[e]sg are distinguished by their near-infrared excess radiation and dusty envelopes which appear to be concentrated in the equatorial region and may obscure much of the star as shown by the SEDs of several in M31 and M33 (Humphreys et al. 2017). There is increasing evidence from studies of individual B[e]sg that they are close, interacting binaries with rapid rotation driven mass loss in the equatorial region (de Wit et al. 2014).

The list of B[e]sg in Table 2 is primarily from Kraus (2019). In the LMC the B[e]sg are found over a range of spectral types and luminosity from early B-type supergiants to late B and early A-type stars. This is similar to what Humphreys et al. (2017) found in M33. Figure 3 shows an HRD diagram with the B[e]sg. Their luminosity distribution clearly suggests a wide range in initial masses for the progenitors of the B[e]sg class with potentially three recognizable groupings by luminosity.

## 2.3. Wolf-Rayet Stars

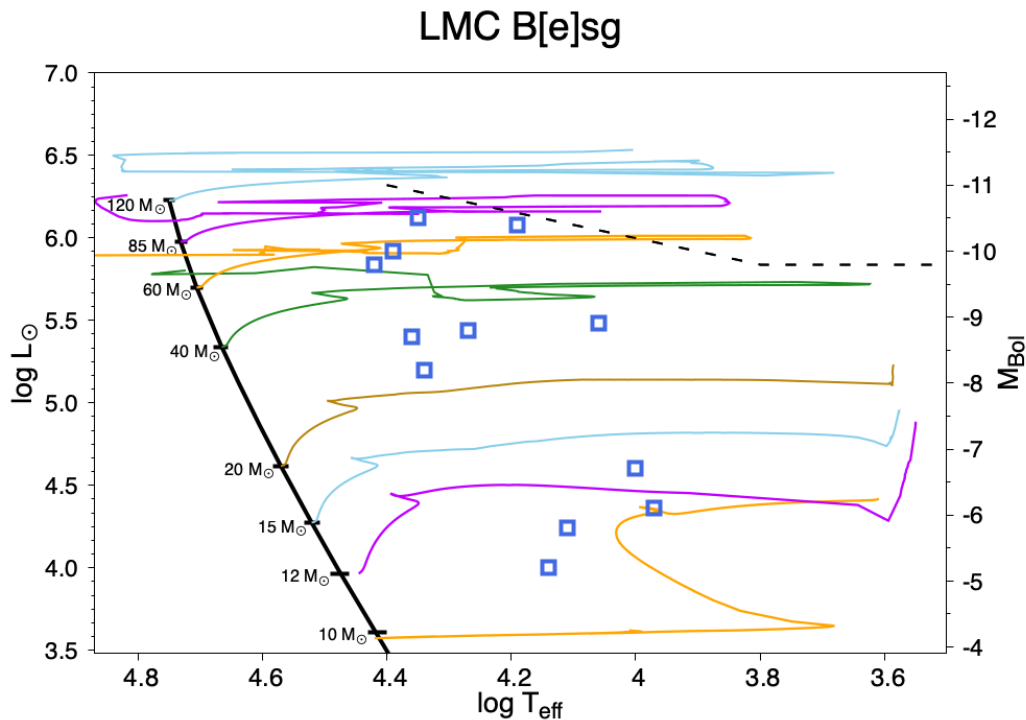


**Figure 3.** An HR diagram of the B[e]sg in the LMC discussed in the text show as blue open squares. The ZAMS and evolutionary tracks are adopted from Eggenberger et al. (2021)  $Z = 0.006$  non-rotating models (LMC is  $Z = 0.004$ ).

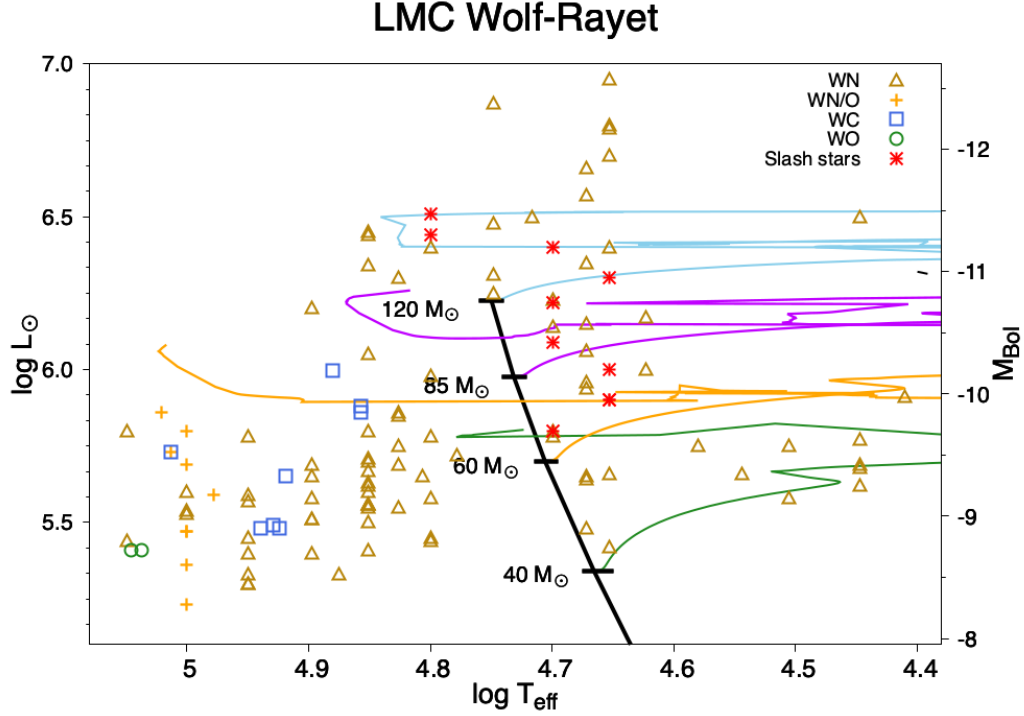


**Figure 4.** An HR diagram of the 126 of 152 WR in the LMC which have published temperature and luminosity (Testor & Niemela 1998; Massey et al. 2000; Bestenlehner et al. 2014; Hainich et al. 2014; Gvaramadze et al. 2014; Neugent et al. 2017; Aadland et al. 2022). WN type are gold triangles. WN3/O3 are orange crosses, WC type are blue squares, WO type are green circles. O2-3If\*/WN "slash stars" are red asterisk. The ZAMS and evolutionary tracks are adopted from Eggenberger et al. (2021)  $Z = 0.006$  non-rotating models (LMC is  $Z = 0.004$ ).

We sorted the list of LMC Wolf-Rayet (WR) stars from Neugent et al. (2018) into five classifications: WN, WN3/O3, Of/WN slash-stars, WC, and WO. The WN and WC stars are separated into high ( $M_{Bol} < -9.7$ ) and less luminous ( $-9.7 \leq M_{Bol} < -8.0$ ) groups. The slash-stars are all high luminosity. The WO and WN3/O3 are predominantly lower-luminosity. Appendix C includes the details for each WR sample in our study. The WR of different types which have published luminosities and temperatures (127 out of 152) are shown on the HR Diagram in Figure 4.

### 3. SPATIAL DISTRIBUTION AND NEAREST NEIGHBOR ANALYSIS

Most of the stars discussed in this paper are post-main sequence. This is clear from their spectroscopic properties; temperatures, luminosities, and positions on the HR Diagram. We should not expect to find them closely associated with main sequence stars. Their appropriate comparison population should be the evolved stars that share the same range of initial masses and ages. On the HR Diagram, we use luminosity as a substitute for mass and temperature or spectral type for age or evolutionary state. In this section we focus on the spatial distribution of each group.

As they age, stars are expected to move from their birthplace. The stars they were born with will do likewise, so we expect an increasingly more dispersed comparison population as the stars age and evolve. For example, the B[e]sgs divide into three groups on the HR Diagram (Figure 3). Based on their positions on the HR Diagram, we expect the most luminous to be associated with mid to late

**Table 3.** Reference Samples

Name	Number	Spectral Types	Median Sep. (pc) <sup>a</sup>
High Luminosity Samples ( $M_{Bol} < -9.7$ )			
Early O-types	38	O2-O4	41
Mid O-types	47	O4.5-O7	24
Late O-types	15	O7.5-O9	329
Early B (high luminosity)	47	O9.2-B2.5	124
Less Luminous Samples for LBVs, B[e]sg, and WR ( $-8.0 > M_{Bol} \geq -9.7$ )			
Early + Mid O-types	212	O2-O7	14
Late O + Early B-types	610	O7.5-B2.5	27
Mid + Late B-Types	76	B3-A0	136
A Supergiants	9	A1-A8	258
Yellow Supergiants (YSG)	22	A9-K4.5	282
Yellow Hypergiants (YHG) <sup>b</sup>	6	A9-K4.5	1367
Red Supergiants (RSG)	45	K5 and later	113
Lowest Luminosity Samples for B[e]sg ( $-5 > M_{Bol} \geq -7$ )			
All O-type + Early B-type	791	O2-B2.5	14
Mid B-type	162	B3-B7	138
Late B-type	324	B7.5-A0	108
A Supergiants	183	A1-A8	125
Yellow Supergiants (YSG)	34	A9-K4.5	437
Red Supergiants (RSG)	109	K5 and later	109

<sup>a</sup>The median separation of the stars in the population from each other computed by performing a nearest neighbor analysis of the population relative to itself.

<sup>b</sup>The yellow hypergiants have circumstellar dust and high mass loss rates which may be due to a post-RSG evolutionary state (Humphreys et al. 2023).

O-type stars, while the least luminous group shares space on the HR diagram with evolved 12 to 15  $M_{\odot}$  stars that may be evolving to the red supergiant stage. The more massive stars that they may have formed with will have already become RSGs or even supernovae.

In the following discussion, we have identified reference populations in the LMC based on their positions on the HR Diagram in Figure 1. The reference samples are initially divided into three groups based on luminosity, a substitute for initial mass: (1) the most luminous, above the H-D limit at  $M_{Bol} < -9.7$  ( $\log(L/L_{\odot}) > 5.7$ ), (2) less luminous stars with  $M_{Bol}$  between -8.0 and -9.7, and (3) a limited group with luminosities  $M_{Bol}$  between -5.0 and -7.0, chosen as a reference sample for the lowest luminosity B[e]sg. Further subdivision is based on spectral types as an indicator of evolutionary state. The reference samples are summarized in Table 3. Six high luminosity yellow hypergiants (YHG) with circumstellar dust and high mass loss (Humphreys et al. 2023) which may be indicative of post-red supergiant evolution, have been separated from the yellow supergiants. Known and suspected binaries are included based on their spectral types

The spatial distribution of the reference samples are shown on large maps in Appendix B. These maps show that the earliest type stars, near the main sequence, are more tightly clustered than those with older evolutionary ages. This demonstrates the importance of comparing our target groups with a reference sample that shares their space on the HR Diagram and are likely to have similar ages.

While many stars with relatively older evolutionary ages tend to be more dispersed, the 30 Doradus region includes at least five distinct stellar groups ranging in evolutionary ages from ongoing star formation to more than 10 Myr old (Walborn & Blades 1997). Thus stars of a more advanced evolutionary age may be found in relatively close projected proximity to much younger stars. The impact this has on the analysis will be discussed.

We present a simple form of nearest-neighbor analysis with cumulative distribution plots like those in the statistical Kolmogorov-Smirnov (K-S) tests. In a nearest neighbor analysis, the relative spacing between members of two different populations is only meaningful if both populations share a characteristic spatial-dispersion size-scale. But, several differing size-scales coexist in the LMC. (1) each star formation region has its own age and velocity dispersion, (2) the velocity dispersion may depend on stellar mass, (3) for some stars the distance from the nearest neighbor,  $D_1$ , is related to the separation between two star formation centers, and (4) the LMC has its own global size scale. The multiple spatial scales complicate the use of the standard K-S test. For these reasons, we measure the dispersion of each reference population relative to itself. Older populations with more time to disperse from their point of origin will tend to have a greater median distance between members (Table 3). The more alike the cumulative distributions are the more likely the sample is drawn from that population.

We measure the distance from the nearest neighbor in the reference populations for each target in our LBV, B[e]sg and WR samples, and compare the results on a cumulative distribution plot. However, caution is called for when using statistics to characterize small samples such as our LBV and B[e]sg targets with only a few stars. Samples smaller than  $N < 20$  cannot yield K-S test results with strong significance (Press et al. 1986) and samples smaller than  $N < 8$  cannot be analyzed with even a one sigma significance. See Davidson et al. (2016) for a detailed discussion about how sampling can influence the nearest neighbor analysis. Hence we have not included any formal K-S tests. We show the cumulative distributions here for visual inspection and for comparison with previous work (Smith & Tombleson 2015; Humphreys et al. 2016; Davidson et al. 2016; Smith 2019) and the recent paper by Deman & Oey (2024).

### 3.1. *The Luminous Blue Variables*

Figures 5 and 6 show the confirmed and candidate LBVs on an H-alpha image of the LMC with the reference populations defined in Table 3. The conclusion is clear. Most LMC LBVs are in the line of sight with known H II regions. They are not isolated from other massive stars. Candidate LBV S61 and less luminous LBV R71 are exceptions. Each is more than 350 pc from the nearest star of comparable luminosity in the reference samples. S61, however, is close to four higher luminosity WN stars (see Figure C2). Candidate LBV S119 is also somewhat isolated, 220 pc from its nearest neighbor of comparable luminosity, but it is also associated with a region northwest of the Tarantula nebula which includes H-alpha emission and many stars with  $-8.0 > M_{Bol} \geq -9.7$  including the less luminous LBV R110. Thus S119 ( $M_{Bol} = -9.8$ ) may be evolved from a less luminous progenitor.



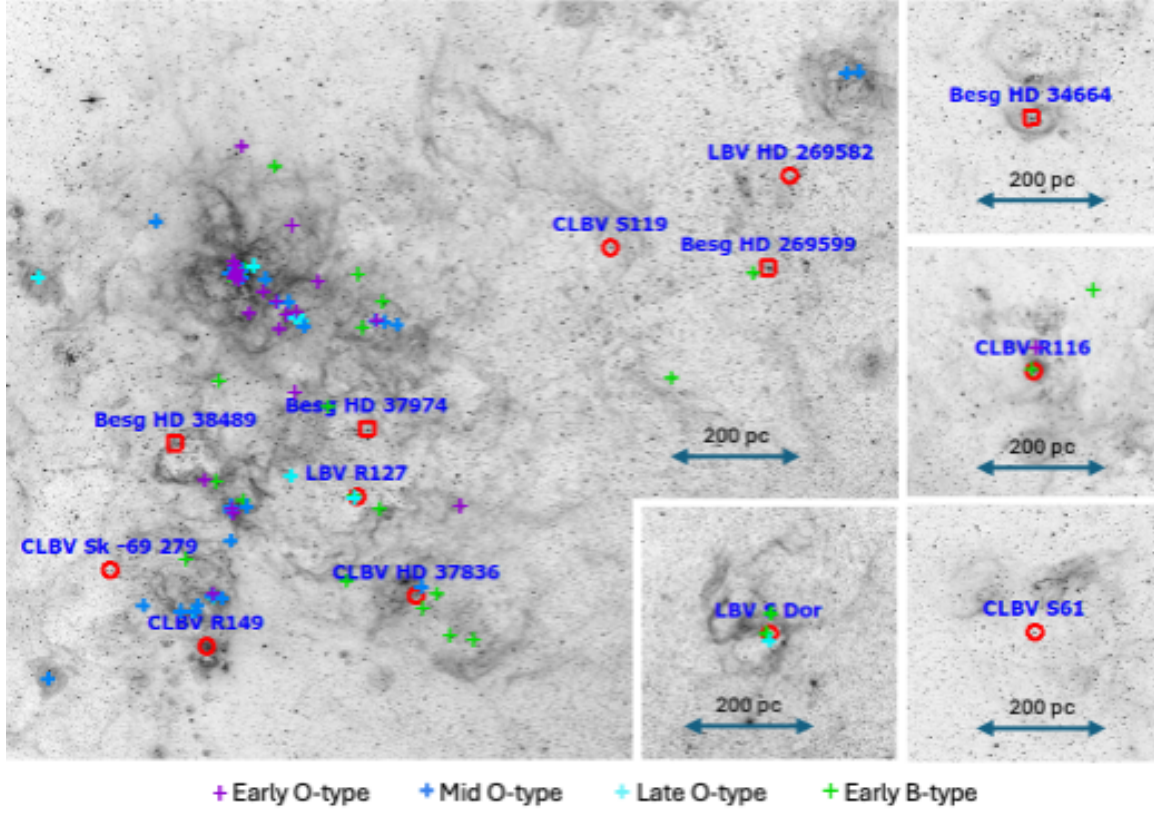


**Figure 5.** The high luminosity ( $M_{\text{Bol}} < -9.7$ ) LBVs, candidate LBVs, and the B[e]sg plotted with red circles on H-alpha emission images of the LMC from MCELS (Smith & MCELS Team 1999). The plots also include the reference samples in the matching luminosity range (Table 3): Early O-types (purple), Mid O-types (blue), Late O-types (cyan), and Early B-types (green).

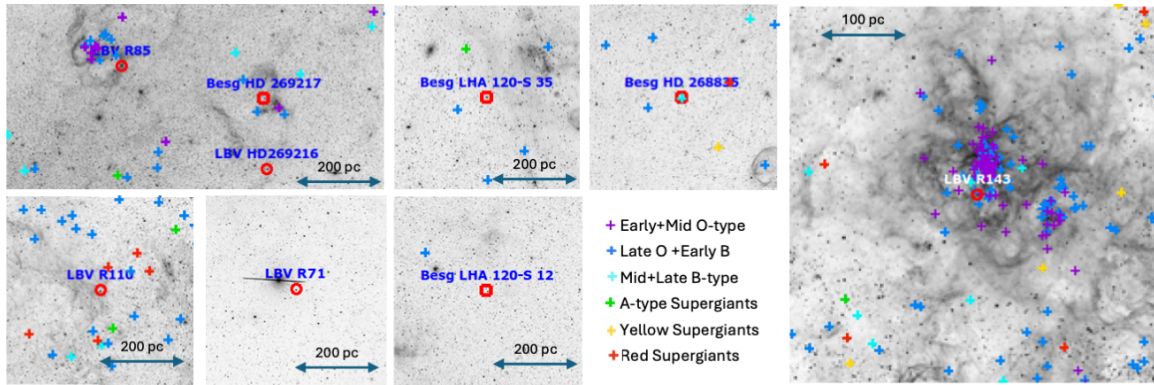


**Figure 6.** The less luminous ( $-9.7 \leq M_{\text{Bol}} < -8$ ) LBVs and the B[e]sg plotted with red circles on H-alpha emission images of the LMC from MCELS (Smith & MCELS Team 1999). The plots also include the reference samples in the matching luminosity range (Table 3): Early + Mid O-types (purple), Late O-types + Early B-types (blue), and Mid + Late B-types (cyan), A-type supergiants (green), yellow supergiants (gold), and red supergiants (red).

### 3.1.1. The Classical (High Luminosity) LBVs

Figure 5 shows the S Dor region and images centered on the classical LBVs together with the stars from the high luminosity ( $M_{\text{Bol}} < -9.7$ ) reference populations in the same projected area. The candidate LBVs are included because they all fall into the high luminosity group. The identification of any H II region or cluster associated with the targets is given in Table 4. S Dor and HDE 269582 are in clusters between 1-6 Myr old (Copetti et al. 1985; Wolf et al. 2007; Popescu et al. 2012; Asa'd et al. 2016). R127 is close to main sequence early O-type stars as well as a 3-6 Myr old cluster containing evolved late O-type and early B-type supergiants (Heydari-Malayeri et al. 2003). The common factor between all three classic LBV is their close proximity to evolved late O-type and early B-type post-main sequence stars. The candidate-LBVs are also associated with evolved late O-type and early B-type supergiants. R149 is in a star cluster with an estimated age of 4-6 Myr (Copetti et al. 1985).

The results of the nearest neighbor analysis (Figure 7) show that the classic LBVs and candidate LBVs best match the distributions of the late O and early B-type supergiants in the same luminosity range. The effect of the small sample size for the classic LBVs is clear. Even though there are only three classic LBVs, they are more closely associated with evolved late-O and early B-type supergiants with evolutionary ages of 2-4 Myr (Eggenberger et al. 2021) rather than with main sequence stars of the same luminosity. The spectral type of the nearest star to each target with similar luminosity (Table 4) reinforces that result.

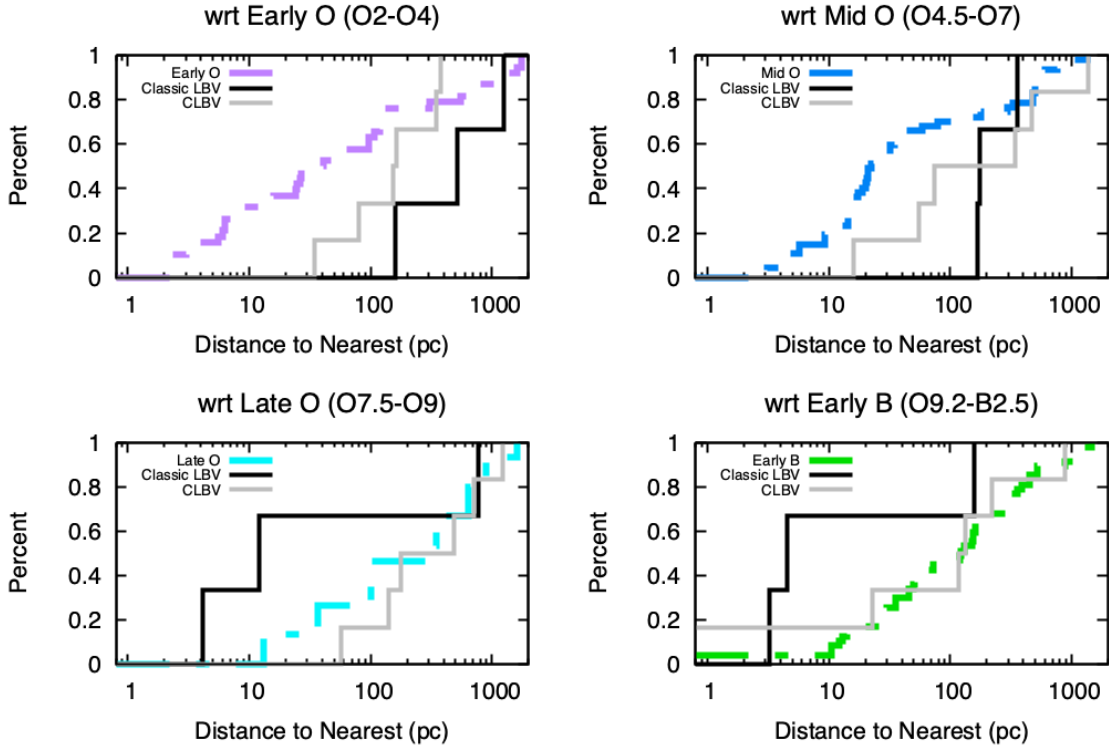


**Figure 7.** Cumulative distribution plots of the nearest neighbors for classic LBV (black) and candidate LBV (gray) plotted relative to high luminosity  $M_{\text{Bol}} < -9.7$  reference samples (colored dotted line).

**Table 4.** Distance to Nearest Neighbors for with Respect to Reference Samples  $M_{Bol} < -9.7$

Star	Early O-type $\alpha$			Mid O-type $\alpha$			Late O-type $\alpha$			Early B-type $\alpha$			In Line of Sight $b$		Age (Myr)	
	D1	D2	D3	D1	D2	D3	D1	D2	D3	D1	D2	D3	Nearest $C$	Name		
	(pc)	(pc)	(pc)	(pc)	(pc)	(pc)	(pc)	(pc)	(pc)	(pc)	(pc)	(pc)	SpType	D(pc)		
Classic LBV																
S Dor (HD 35343)	1236	1297	1383	359	746	756	12	360	1198	3	28	282	O9.5	3	H88-267, LHA-120 N119, DEM L132a	1-6 <sup>1</sup>
HDE 269582 (Sk -69 142a)	520	669	714	171	192	193	776	786	796	158	497	547	B0	158	LH 61, NGC 1983	1-6 <sup>2</sup>
R 127 (HDE 269858)	159	184	189	177	190	642	4	103	268	5	42	130	O8.5	4	NGC 2055	3-6 <sup>3</sup>
Candidate LBV																
S119 (HD 269687)	373	447	456	346	363	376	482	493	544	220	223	357	B0	220	BSDL 2141	-
R 116 (HD 269700)	35	598	617	472	490	655	704	720	724	0	153	576	B1.5	0	LHA 120-N 148	-
HD 37836	152	302	307	16	291	292	175	261	308	23	33	81	O6	16	LHA 120-N 154	-
R 149 (Sk -69 257)	80	205	212	55	62	65	57	76	289	135	227	236	O6	55	NGC 2083, LHA 120-N 159	4-6 <sup>4</sup>
Sk -69 279	162	197	206	73	125	143	142	161	310	117	208	209	B1	117	[GKK2003] O161	-
S61 (Sk -67 266)	344	891	941	1369	1604	1627	1221	1623	1732	875	920	922	O3	334	[KDS99] GS 94, DEM L 308	-
High Luminosity B[e]sg																
HD 34664 (B0/0.5I[e])	1447	1506	1520	522	814	839	766	1549	1579	299	1038	1097	B1	299	NGC 1871, LHA 120-N 30	-
HD 269599 (B1)	596	617	683	316	327	571	712	724	724	23	224	588	B0	23	NGC 1994 (BSDL 1890)	6-9 <sup>5</sup>
HD 37974 (B0.5e)	123	164	185	164	164	164	105	135	191	67	105	125	B0	67	NGC 2050 (BSDL 2554)	-
HD 38489 (B0)	71	131	139	128	132	144	183	240	256	86	86	116	O4	71	NGC 2081	3-4 <sup>4</sup>

<sup>a</sup>Reference samples include stars in the same luminosity range ( $M_{bol} < -9.7$ ). D1, D2, and D3 are distances to the first, second, and third nearest stars in the reference sample in parsecs.

<sup>b</sup>Determined using Bica et al. (2008).

<sup>c</sup>Spectral type and distance in parsecs of the nearest other star in the same luminosity range.

<sup>1</sup>Copetti et al. (1985), Hunter et al. (2003), Wolf et al. (2007), and Popescu et al. (2012)

<sup>2</sup>Hunter et al. (2003), Wolf et al. (2007), Popescu et al. (2012), and Asa'd et al. (2016)

<sup>3</sup>Heydari-Malayeri et al. (2003)

<sup>4</sup>Copetti et al. (1985)

<sup>5</sup>Copetti et al. (1985), Cassatella et al. (1996), and Wolf et al. (2007)

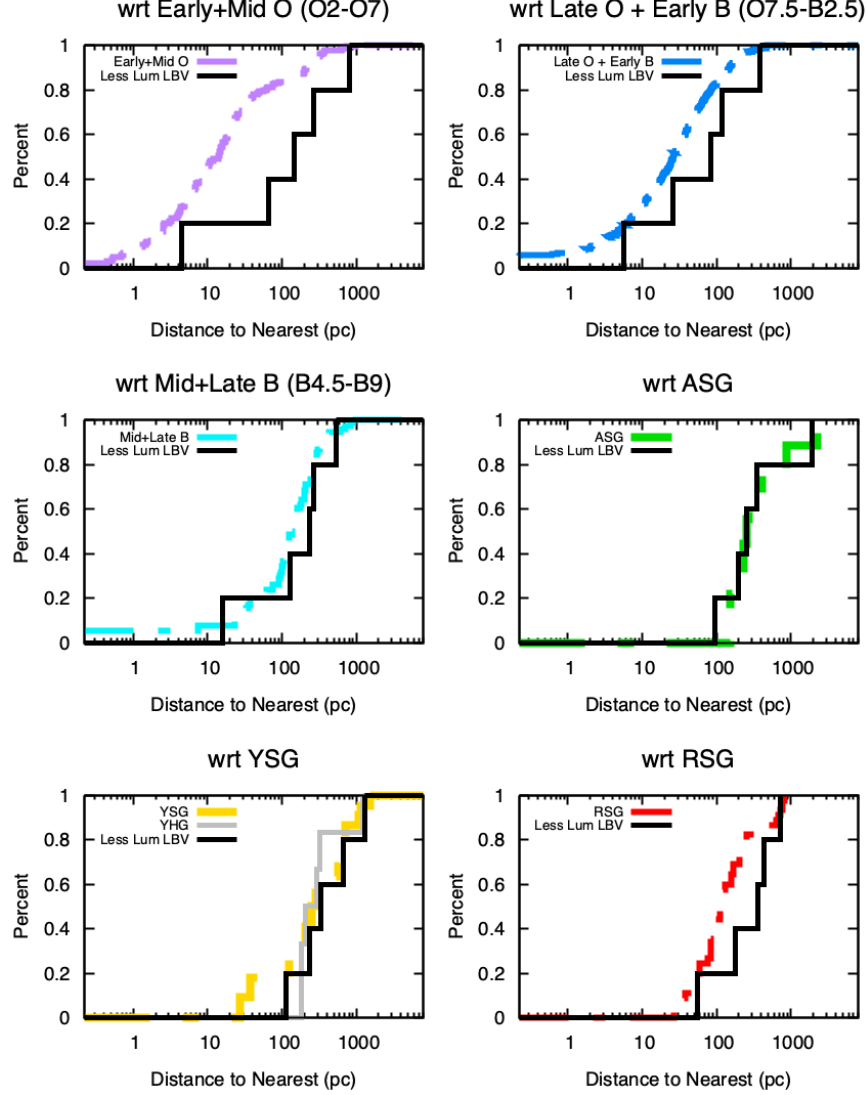


**Figure 8.** Cumulative distribution plots of the nearest neighbors for the less luminous LBVs (black) plotted relative to mid luminosity  $-8.0 > M_{Bol} \geq -9.7$  reference samples (colored dotted line). The YHG sample is also plotted relative to the YSG as a gray line in that panel.

### 3.1.2. *Less Luminous LBVs*

Figure 6 shows images centered on the less luminous LBVs with stars of similar luminosity ( $-8.0 > M_{Bol} \geq -9.7$ ). In this luminosity range the main sequence corresponds to early and mid O-type stars. As with the highest luminosity LBVs, a few are close to main sequence stars of similar luminosity while others are more isolated. All but one are found close to evolved B-type stars. R71 is isolated from every type of star in the same luminosity range. R85 is in the southwest part of the large spiral shaped emission nebula LHA-120 N119 and OB association NGC 1910 (LH 41) which includes at its heart several evolved supergiants including LBV S Dor. R110 resides in an area just northwest of the Tarantula Nebula which includes relatively few high luminosity stars (Figure B1) but many stars of comparable luminosity including several RSG, one WN, and one WC, implying a mix of evolved stars more than 3 Myr old.

**Table 5.** Distance to Nearest Neighbors with Respect to Reference Samples  $-8.0 > M_{Bol} \geq -9.7$

Star	Late O + Early B <sup>a</sup>			Mid + Late B <sup>a</sup>			ASG <sup>a</sup>			YSG <sup>a</sup>			Nearest <sup>c</sup>		In Line of Sight <sup>b</sup>	Age (Myr)
	D1	D2	D3	D1	D2	D3	D1	D2	D3	D1	D2	D3	D3	D(pc)		
	(pc)	(pc)	(pc)	(pc)	(pc)	(pc)	(pc)	(pc)	(pc)	(pc)	(pc)	(pc)	(pc)	SpType	Name	
Lower Luminosity LBV																
R 71 (HDE 269006)	388	399	408	530	587	974	1912	2755	2758	1288	1595	1842	-	B0	388	-
HDE 269216 (Sk -69 75)	118	134	134	234	281	411	346	1159	1277	336	995	1188	LH 39, BSDL 940	O8.5	118	-
R85 (HDE 269321)	26	50	64	265	311	333	255	755	881	681	739	799	NGC 1910, LHA-120 N 119, DEM L132b	B0.5	26	-
R 110 (HDE 269662)	83	96	99	126	168	199	94	225	370	237	249	324	-	RSG	56	-
R 143	6	12	14	16	16	17	196	351	514	115	167	246	30 Dor, see text	O5	6	2-3 <sup>d</sup>
Mid Luminosity B[e]sg																
HD 269217 (B5/6Ia[e])	35	61	64	101	126	302	1620	2401	2530	142	567	584	LH 35, LHA 120-N 113	O8	35	6-7 <sup>d</sup>
LHA 120-S 12 (B0.5Ie)	168	429	431	578	764	782	2288	2572	2731	611	1181	1270	-	B0.5	168	-
HD 268835 (B8[e])	83	156	216	0	243	512	384	1083	1213	409	994	1134	-	B8	0	-
LHA 120-S 35 (Hot)	73	154	184	400	658	695	121	2188	2216	741	901	912	KMHK 915 = [SL63] 482	B0.5	73	10-30 <sup>d</sup>

<sup>a</sup>Reference samples include stars in the same luminosity range ( $-8.0 > M_{Bol} \geq -9.7$ ). D1, D2, and D3 are distances to the first, second, and third nearest stars in the reference sample in parsecs.

<sup>b</sup>Determined using Bica et al. (2008).

<sup>c</sup>Spectral type and distance in parsecs to the nearest other star in the same luminosity range.

<sup>1</sup>Walborn & Blades (1997)

<sup>2</sup>Copetti et al. (1985)

<sup>3</sup>van Loon et al. (2005) and Torres et al. (2018)



R143, now considered a less luminous LBV, (see section 2.1) is in the 30 Dor region (Figure 5) surrounded by a mixed population of evolved stars ranging from O to mid B-type supergiants with a likely age of 2-5 Myr (Walborn & Blades 1997). The closest stars to R143 do not have published spectral types. We use their published photometry with the Q-method to estimate their intrinsic colors and visual extinctions. The  $A_v$  for R143 (Agliozzo et al. 2019) is less than for the probable O-type stars and more like that for the candidate B-type supergiants. R143 is therefore likely projected in front of the younger O-type stars, and associated with the B-type supergiants.

Figure 8 and Table 5 show the results of the nearest-neighbor analysis of the less luminous LBVs compared to reference samples with  $-8.0 > M_{Bol} \geq -9.7$ . The less luminous LBVs have a distribution consistent with the evolved A-type supergiants (ASG) and yellow-supergiants (YSG) of the same luminosity class. Note also their similarity with the yellow hypergiants which may be post-RSGs.

The less luminous LBVs range in luminosity from  $-9.7 \leq M_{Bol} \leq -8.5$  corresponding to evolved stars with masses between  $30 - 40 M_{\odot}$  and ages from 4.5 - 6 Myr (Eggenberger et al. 2021). The evolutionary tracks show that the late B-type stars and A supergiants in this luminosity/mass range may spend roughly twice as much time on post-RSG blue evolutionary loops as they do during the post main sequence first crossing. Both evolutionary states occupy the same temperature and luminosity range so this analysis cannot distinguish between them.

### 3.2. B[e]sg

The HR-Diagram of the B[e]sg (Figure 3) has three clear groupings by luminosity with four in each group; highest luminosity B[e]sg ( $M_{Bol} < -9.7$ ), mid-luminosity ( $-9.7 \leq M_{Bol} < -8$ ), and the lowest luminosity ( $M_{Bol} \geq -7$ ).

The highest luminosity B[e]sg ( $M_{Bol} < -9.7$ ) have spectral types between B0 – B1. Plots of the area around each show that all four are in proximity to evolved early B-type stars (Figure 5). HD 269599 is close to the center of NGC 1994 which has an estimated age between 7 - 16 Myr (Hodge 1983; Cassatella et al. 1996; Kumar et al. 2008; Glatt et al. 2010) and contains a few YSG and RSG (Humphreys 1979; Frogel & Cohen 1982). HD 37974 appears to be a member of star cluster NGC 2050 (LH 93) which contains no early O-type stars and several mid and late O-type and early B-type stars (Hill et al. 1994). HD 38489 is close to cluster LH 104 with an estimated age of 3-5 Myrs (Tarrab 1985). So even though HD 37974 and HD 23489 are close in projection to early O-type stars they are also closely associated with more evolved populations. Figure 9 and Table 4 show the results of the nearest neighbor analysis agree well with the spatial distribution maps. The highest luminosity B[e]sg have a distribution that is most similar to post-main sequence early B-type supergiants in the same luminosity range like the classic and candidate LBVs.

The mid luminosity B[e]sg ( $-9.7 \leq M_{Bol} < -8$ ) include a wider range of spectral types (B0 to A0). Spatial plots show that three of the four mid-luminosity B[e]sg are well separated from any early O-type stars (Figure 6). The exception, HD 269217, is on the edge of stellar association LH 35 which has an estimated age less than 10 Myr (Copetti et al. 1985; Bica et al. 1996). LHA 120-S-35 is associated with cluster KMHK 915 which has an estimated age of 10-30 Myr (van Loon et al. 2005; Torres et al. 2018). All four are in relative proximity to early B-type stars and LHA 120-S 35 and HDE 268835 are also close to A-supergiants, YSG, and RSG of similar luminosity. Figure 10 and Table 5 show the results of the nearest neighbor analysis. Their cumulative distributions show that



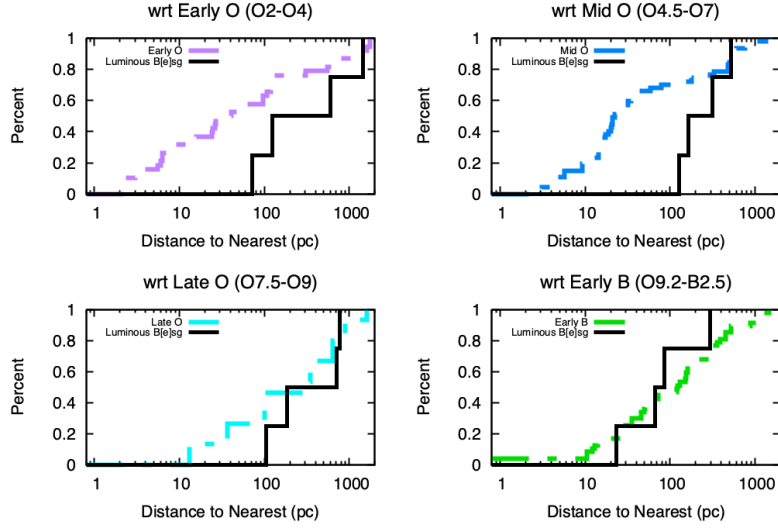


**Figure 9.** Cumulative distribution plots of the nearest neighbors for the highest luminosity B[e]sg (black) plotted relative to the high luminosity  $M_{Bol} < -9.7$  reference samples (colored dotted line).

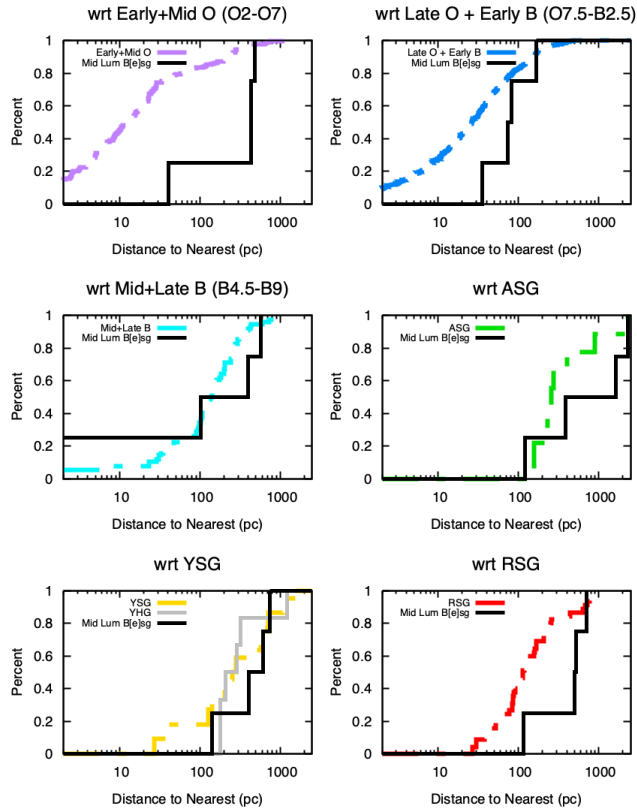


**Figure 10.** Cumulative distribution plots of the nearest neighbors for mid-luminosity B[e]sg (black) plotted relative to the mid luminosity  $-8.0 > M_{Bol} \geq -9.7$  reference samples (colored dotted line). The YHG sample is also plotted relative to the YSG as a grey line in that panel.

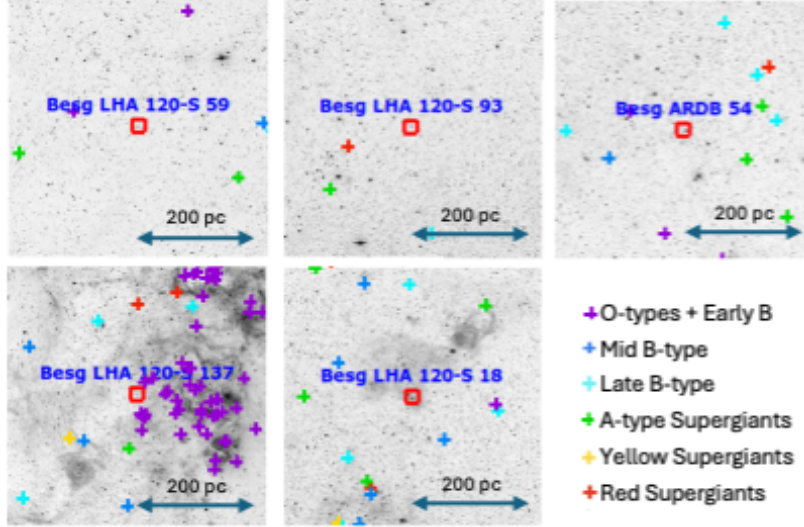


**Figure 11.** The lowest luminosity B[e]sg plotted on H-alpha emission images of the LMC from MCELS (Smith & MCELS Team 1999). The plots also include the reference samples in the matching luminosity range (Table 3): O-types and Early B-Types (purple), Mid B-types (blue), Late B-types (cyan), A-type supergiants (green), yellow supergiants (gold), and red supergiants (red)..

**Table 6.** Distance to Nearest Neighbors for Lowest Luminosity B[e]sg

Star	Sp Type	Mid B-type <sup>a</sup>			Late B-types <sup>a</sup>			Nearest <sup>b</sup>	In Line of Sight <sup>c</sup>	
		D1	D2	D3	D1	D2	D3			
		(pc)	(pc)	(pc)	(pc)	(pc)	(pc)	SpType	D(pc)	Name
ARDB 54	A0-II	134	244	277	153	156	192	B1	94	KMHK 264
LHA 120-S 93	A0:I:	257	346	403	184	285	317	B8	184	-
LHA 120-S 59	B0.5IIIe	117	188	197	140	176	258	B1.5	25	-
LHA 120-S 137	BlaePCyg	210	382	481	227	284	310	B1	111	-

<sup>a</sup>Reference samples only include stars in the same luminosity range  $M_{Bol} \geq -7$ . D1, D2, and D3 are distances to the first, second, and third nearest stars in the reference sample in parsecs.

<sup>b</sup>Spectral type and distance in parsecs to the nearest star in the same luminosity range.

<sup>c</sup>Determined using Bica et al. (2008).

the mid luminosity B[e]sg are dispersed similar to other post-main sequence samples. Although there is not a strong match the correlation is best with the late B-type supergiants.

The lowest luminosity B[e]sg ( $-7 \leq M_{Bol} < -5$ ) range in spectral type from mid B-type to A0. Note that we did not select for stars in this luminosity range for our HRD. Therefore, the reference samples are incomplete especially for the A-type and yellow and red supergiants at these luminosities. The spatial map comparing the distribution of lowest luminosity B[e]sg shows that they are mostly isolated with the exception of LHA 12-S-137 (Figure 11), which is on the edge of association LH 108,

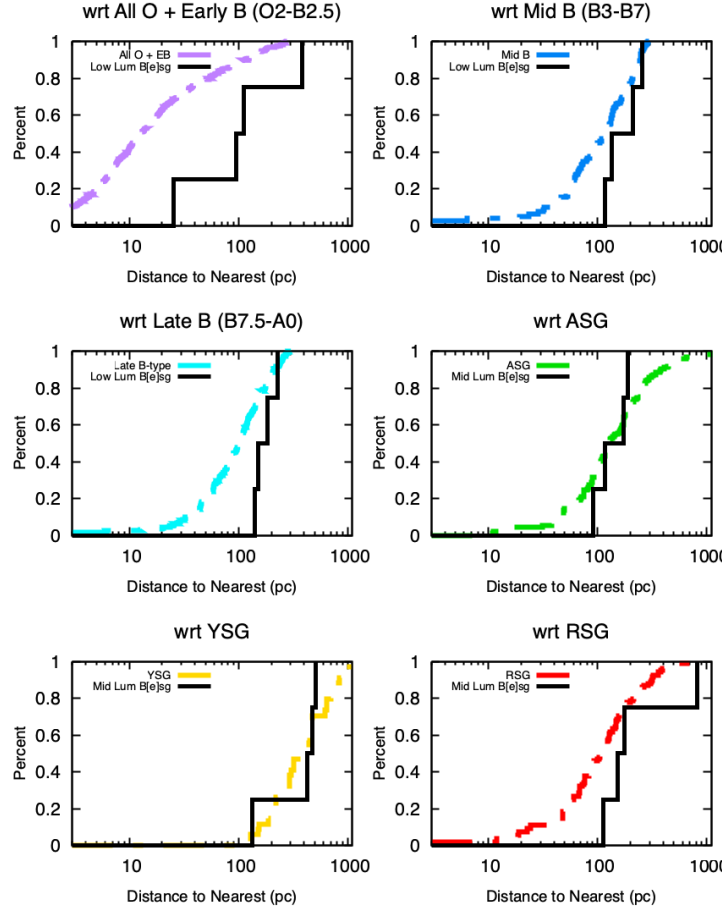


**Figure 12.** Cumulative distribution plots of the nearest neighbors for low-luminosity B[e]sg (black) plotted relative to different lowest luminosity  $-7.0 \leq M_{\text{Bol}} < -5.0$  reference samples (colored dotted line).

and close to late O-type and early B-type main sequence stars. ARDB 54 is associated with star cluster KMHK 264 which has an estimated age between 9-32 Myr (Hunter et al. 2003; Glatt et al. 2010; Popescu et al. 2012). The nearest neighbor analysis is shown in Table 6 and Figure 12. The nearest star for each of the lowest luminosity B[e]sg are B-type stars close in spectral type to the target itself. The distribution of the lowest luminosity B[e]sg relative to each reference sample best matches the A-supergiants and YSG.

### 3.3. Wolf-Rayet Stars

Wolf-Rayet stars are found predominantly near other luminous stars and in the line of sight with young clusters and H II regions (Figures 17, 18, C1, and C2). This is consistent with the theory of WR as O-type stars which have been stripped of their hydrogen envelope (Conti 1996). Meynet & Maeder (2005) predict that at the metallicity of the LMC, the minimum mass for a WR progenitor in single star evolution is about  $20 M_{\odot}$  although, lower mass stars may become WR through binary interaction. The same modeling also supports the possibility that some single star WR may become RSGs prior to entering their WR phase. As a result, WR should be dispersed similar to other massive stars which have evolved past the main sequence including possible post-RSG evolution. In the following discussion, we treat each subgroup of WR stars separately.

3.3.1. *WN Stars*

The comparison between the WN samples and the reference populations is robust because there are several dozen stars in each set. The late WNs are considered to be the entry point to the WR sequence, and over time as they lose more of their hydrogen envelope, they evolve to the earlier type, hotter WNs (Conti et al. 1983; Hamann et al. 1991). The hotter early-type WNs may be more evolved or have been in the WR state longer than the later types with more hydrogen in their spectra. Thus the early and late WN stars may have different ages and different distributions.

We separated the high luminosity WNs by type into early (WN3 - WN4.5) and late (WN5 - WN7) with 19 and 18 stars, respectively. Figure C2 shows that the late WNs are highly concentrated in the 30 Doradus region while the early WN's are more spatially dispersed. The early WN's have a median separation of 289 pc relative to each other, which is comparable to the late O-type supergiants of the same luminosity (median separation of 329 pc, Table 3). Figure 13 confirms that the early WN's have a spatial distribution similar to evolved late O-type supergiants. The late WN's, however, do not share the spatial dispersions of any of the high luminosity O stars or early B supergiants. They have a median separation of 7.5 pc relative to each other, much more concentrated than even the early and mid O-types of the same luminosity (41 pc and 27 pc respectively in Table 3). This peculiar result is probably a consequence of their concentration in one region, 30 Dor, and reflects the cautionary remarks at the beginning of Section 3 about size-scales in the LMC.

Figure 14 shows the nearest neighbor distribution of the 63 less luminous WN split into earlier types (WN2-WN4) with 46 members and later types (WN5-WN11) with 17 stars. Both samples

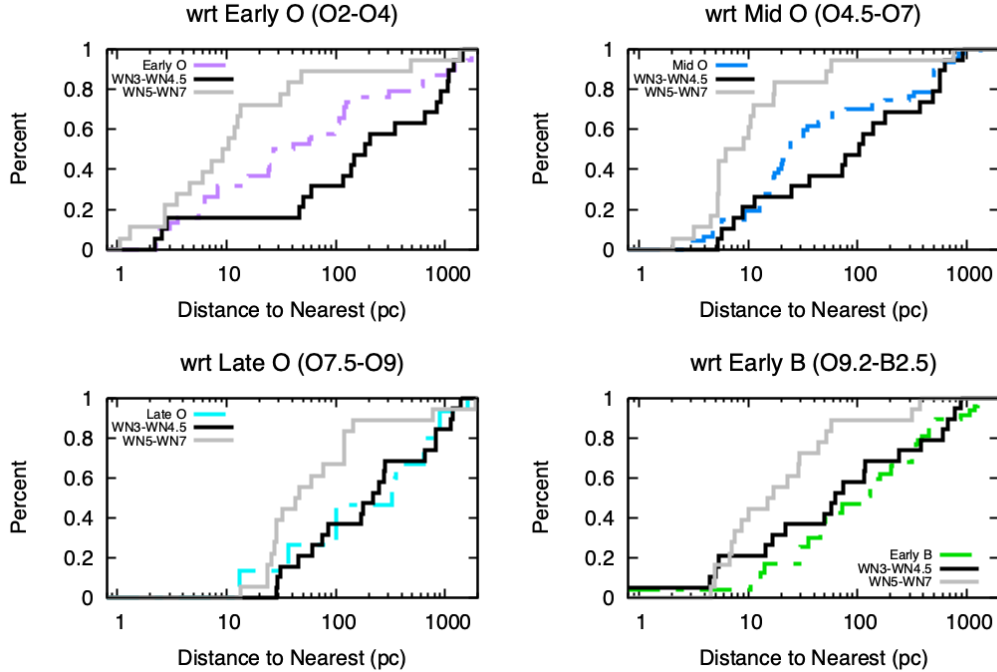


**Figure 13.** Cumulative distribution plots of the nearest neighbors for the highest luminosity WN separated into groups by early types (WN3 - WN4.5, black) and later types (WN5 - WN7, gray). Each sample is plotted relative to different high luminosity  $M_{Bol} < -9.7$  reference samples (colored dotted line).

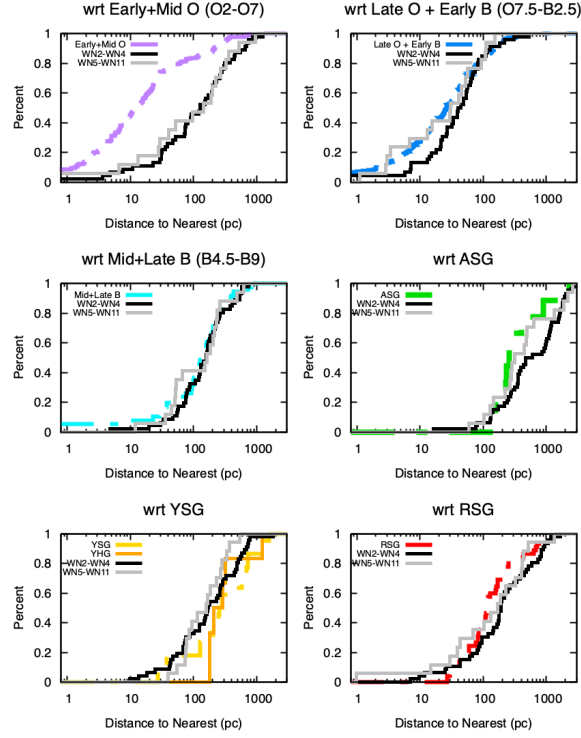


**Figure 14.** Cumulative distribution plots of the nearest neighbors for the less luminous WN separated into groups by early types (WN2 - WN4, black) and later types (WN5 - WN11, gray). Each sample is plotted relative to different mid luminosity  $-8.0 > M_{Bol} \geq -9.7$  reference samples (colored dotted line).

have similar spatial dispersions and compare favorably with the evolved supergiants from late B-type to the red supergiants. Together all 63 less luminous WN have a median separation of 150 pc with respect to themselves, which is comparable to the median separation of similar luminosity mid + late B-types with respect to themselves (136 pc, Table 3).

Neugent et al. (2018) suggested that WN3/O3 stars represent a transitional state between early O-type stars with hydrogen envelopes and full-fledged WN. All the known WR stars of this sub-type are found in the LMC. Figure C1 shows that WN3/O3 are usually found in proximity to the less luminous WN and spread over the whole area of the LMC. This supports the finding by Neugent et al. (2018) that WN and WN3/O3 are closely associated and could be drawn from the same population.

### 3.3.2. WC Stars

The WC Wolf-Rayet stars are considered to be more evolved than WN because their spectra show the products of helium fusion (Gamow 1943; Lamers et al. 1991), while the WN stars show the products of the CNO process. There are two WC stars in our sample with luminosities that place them only slightly above the HD limit. We therefore treat all 23 WC as a single population for comparison with the mid-luminosity reference samples  $-8.0 > M_{Bol} \geq -9.7$  (Table 3). The mean separation between the WC with respect to each other is 162 pc, more than the mean separation of the mid + late B-types (136 pc) and RSG (113 pc) but less than the ASG (258 pc) and YSG (282 pc) in the same luminosity range.

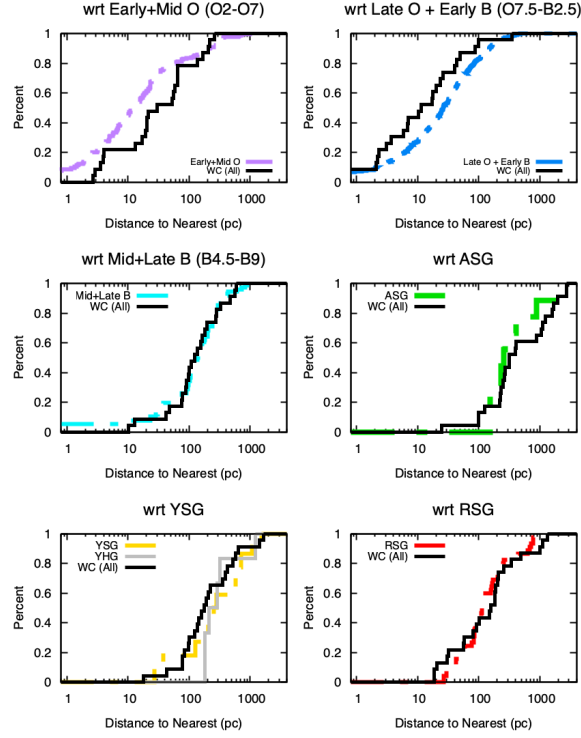


**Figure 15.** Cumulative distribution plots of the nearest neighbors for all 23 WC (black) plotted relative to different mid luminosity  $-8.0 > M_{Bol} \geq -9.7$  reference samples (colored dotted line). The YHG sample is also plotted relative to the YSG as a gray line in that panel.

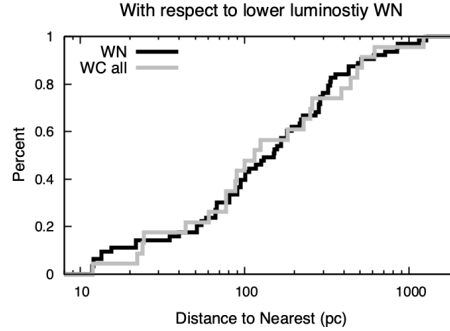


**Figure 16.** Cumulative distribution plots of the nearest less luminosity  $-8.0 > M_{Bol} \geq -9.7$  WN neighbors for the WN themselves (black), and all 23 WC (gray).

Figure 15 compares the full sample of 23 WC to the reference populations between  $-8.0 > M_{Bol} \geq -9.7$ . The distribution of the WC stars is interestingly consistent with the distribution of four evolved populations, the late B-type stars and the ASG, YSG, and RSG distributions. A comparison of WN and WC directly with each other (Figure 16) shows that they have very similar spatial distribution relative to the less luminous WN stars demonstrating that they have probably been drawn from the same population. The WCs could be a post WN stage with one or both phases being relatively short lived so that the older phase does not have time to disperse significantly relative to the younger.



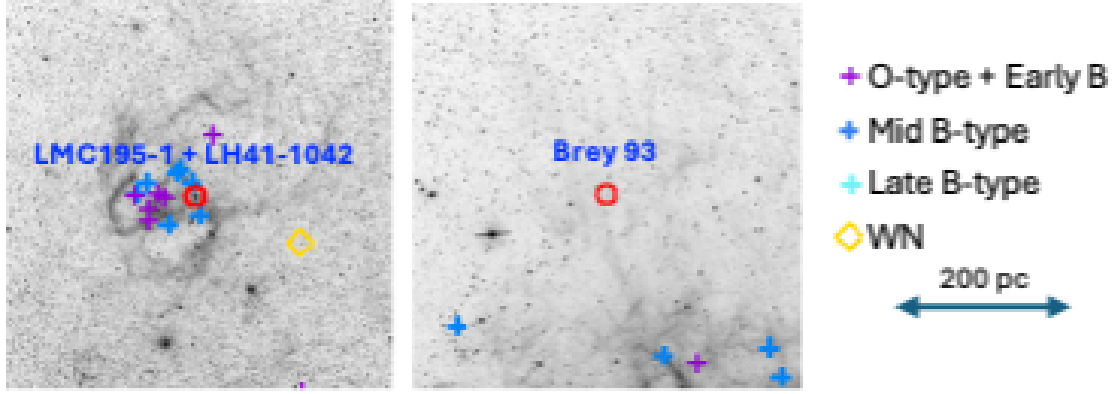


**Figure 17.** The WO plotted with red circles on H-alpha emission images of the LMC from MCELS (Smith & MCELS Team 1999). The plots also include the reference samples in the  $-9.7 \leq M_{Bol} < -8$  luminosity range (Table 3): Early + Mid O-types (purple), Late O-types + Early B-types (blue), and Mid + Late B-types (cyan), and lower luminosity WN (gold diamonds). There are no A-type supergiants, yellow supergiants, red supergiants or WC stars within the bounds of the area plotted around the WO stars.

Recall from Figure 14 that the less luminous WNs are not as well matched to the ASG and RSG spatial distributions as the WC, supporting the expectation that WC are a later phase than WN.

### 3.3.3. WO Stars

The three LMC WO ( $-8.3 < M_{Bol} < -8.7$ ) are best compared with the mid-luminosity reference samples (Table 3). Unfortunately, there are too few WO for a meaningful nearest neighbor analysis. Figure 17 shows mid-luminosity reference stars and WR within 200 pc of each of the LMC WO stars. [MNM2014]LMC195-1 and [L72]LH41-1042 are extremely close to each other and nearby several mid B-type stars of similar luminosity, the high luminosity LBV S Doradus and cluster LH 41. Brey 93 is to the northeast of the Tarantula Nebula, isolated from all other stars in the same luminosity range. Aadland et al. (2022) suggests that WO stars are evolved WC stars reaching the end of a continuous sequence of evolution from late WC to early WO. However, there are no WC within 200 pc of the LMC WO stars. The nearest neighbor analysis of WC show that they have a spatial distributions similar to the later-type evolved supergiants, while [MNM2014]LMC195-1 and [L72]LH41-1042 are associated with several evolved B-type stars but there are no nearby later-type supergiants. This could be a chance superposition. Brey 93 is isolated which could support a more advanced state but it is difficult to tell since there only three WO in the LMC.

### 3.3.4. "Slash" Stars

The Of/WN "slash" stars have a composite spectral classification with an early-type O star and a late WN. Figure 18 shows that they are associated with H-alpha emission and in proximity to WN's and other high luminosity stars. The slash stars are the least dispersed of the WR samples with 8 out of 13 tightly grouped in the heart of 30 Doradus within a projected area fewer than 10 pc across. Normally a small sample may have a large median separation because they would be widely

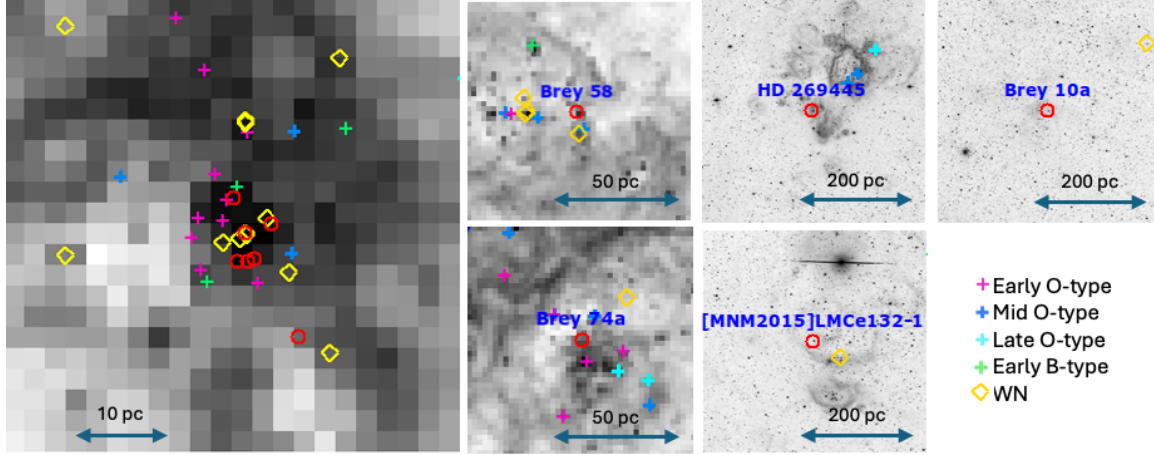


**Figure 18.** The Of/WN slash stars plotted with red circles on H-alpha emission images of the LMC from MCELS (Smith & MCELS Team 1999). The WN stars are plotted as gold diamonds. The plots also include the reference samples in the matching luminosity range ( $M_{\text{Bol}} < -9.7$ ): Early O-types (purple), Mid O-types (blue), Late O-types (cyan), and Early B-types (green). Note the different spatial scales in each section. The image on the far left is a zoom in on the 30 Doradus star forming region.

scattered across the galaxy. Due to their concentration in 30 Dor, their median separation relative to each other is only 4 pc, significantly less than 41 pc for early O-type supergiants and 24 pc for mid O-type supergiants in the same luminosity range (Table 3).

All but two of the slash stars (Brey 10a and HD 269445) are within 50 pc of higher luminosity WNs, and except for [MNM2015]LMCe132-1, the nearest WN is a later type (WN5-WN11). The close association with later type WN is consistent with the sequence proposed by Crowther & Walborn (2011) which identify the slash stars as a transitional stage between the main sequence and late-WN for very massive stars ( $180 - 120 M_{\odot}$ ).

The highly concentrated distribution of slash stars may indicate youth compared to the main sequence stars with the same luminosity. Their high density in 30 Doradus suggests they could be influenced by the exceptional nature of that star forming region. Or there could be a selection bias causing the sample of Of/WN in the LMC to be incomplete if these stars are primarily found at the unresolved hearts of star forming regions.

#### 4. SUMMARY AND DISCUSSION

In this paper we have examined the spatial distributions of evolved massive stars, the LBVs and B[e]sgs and the different subgroups of Wolf-Rayet stars. The B[e]sg, LBVs, and Wolf-Rayet phenomena are all observed across a wide range of luminosities on the HR Diagram implying that stars with different initial masses may exhibit the associated features and characteristics of the different groups at different stages in their post-main sequence evolution.

The classic LBVs, the LBV candidates, the most luminous B[e]sgs and the high luminosity WN stars, have luminosities that place them above the H-D limit at  $M_{\text{Bol}} \approx -9.7$  ( $\text{Log } L/L_{\odot} \approx 5.8$ ), see Figures 2–4, with likely initial masses above  $40 M_{\odot}$ . Their spatial distributions in Figure 5, show that the three classic LBVs are observed projected towards H II regions and young clusters. Candidate LBVs are also observed near young clusters and emission regions except for S61 which

appears relatively isolated. The high luminosity B[e]sg are similarly associated with regions of young stars.

Although the nearest neighbor analysis for the classic LBVs is limited to only three stars, they and the CLBVs have spatial dispersions that are more consistent with the distribution of the luminous late O-type stars and early B-type supergiants. The B[e]sgs are also most closely associated with the early B-type supergiants, consistent with their early B-type spectral types. Their positions on the HRD (Figures 2 and 3) support a post main sequence state for the classic LBVs and the high luminosity B[e]sg. The well known nitrogen and helium-rich ejecta of the LBVs is also strong support for their possible post-CNO cycle state. They may already be in He-burning. In contrast, the nearest neighbor analysis of the the highest luminosity WN stars show mixed results.

The spatial distribution and nearest neighbor analysis yields some interesting results for the LBVs, and B[e]sg below the H-D limit in the luminosity range from  $M_{Bol}$  -8.0 to -9.7 mag, corresponding to an initial mass range from  $\approx 25 - 40 M_{\odot}$ . Based on the positions of the less luminous LBVs and B[e]sg on the HR Diagram we expect them to be post-main sequence stars older than their more luminous, more massive counterparts and likely more dispersed than O and early B-type stars of similar mass and luminosity. The space distribution of both groups (Figure 6) confirms that they are more dispersed and associated with more evolved supergiants. The LBV R71 and the B[e]sg LHA 120 S-12 appear to be the most isolated. The nearest neighbor analysis of the less luminous LBVs is consistent with their appearance in the spatial distribution map and with the distributions of evolved A-type supergiants and yellow supergiants (Figures 8 and 10). Interestingly, their distribution bears a resemblance to the distribution of post-RSGs yellow hypergiants in the YSG panel of Figure 8. The cumulative distribution of the less luminous B[e]sg, is also similar to the more evolved late B supergiants, A-type and yellow supergiants, although the correlation is not as strong as for the less luminous LBVs.

Evolutionary tracks for stars in this luminosity and mass range (Eggenberger et al. 2021) show that they may cross the region of the evolved yellow and blue supergiants more than once. They may spend as much time on a post-RSG blue loop as on their first crossing of the HR Diagram. Both evolutionary states occupy the same temperature and luminosity locus, and although this analysis is not adequate to distinguish them, the less luminous LBVs may be post-RSGs.

The lower luminosity B[e]sg are the lowest luminosity group included in this study. Their luminosities correspond to initial masses of  $10 - 12 M_{\odot}$ . Their spatial distribution show that they are mostly isolated and their nearest neighbor distributions are, not surprisingly, most similar to the A-type and yellow supergiants of the same luminosity. At these masses and luminosities, the stars are not expected to have high line-driven mass loss like luminous O and B-type stars or experience high mass loss episodes like the LBVs. Thus their dusty envelopes and evidence for mass loss may be the consequence of rapid rotation or binarity

As discussed earlier, the evolutionary state of the B[e]sg is open for debate. Their wide range of luminosities suggests the cause of their common observed properties is not a strong function of their mass or luminosity. Their dusty equatorial regions may be due to rotation or binarity or both. Clearly the most luminous B[e]sg in our sample have not been RSGs. The mid-luminosity B[e]sg however are dispersed similarly to the evolved late B-type, A-type, and yellow supergiants. They appear to be

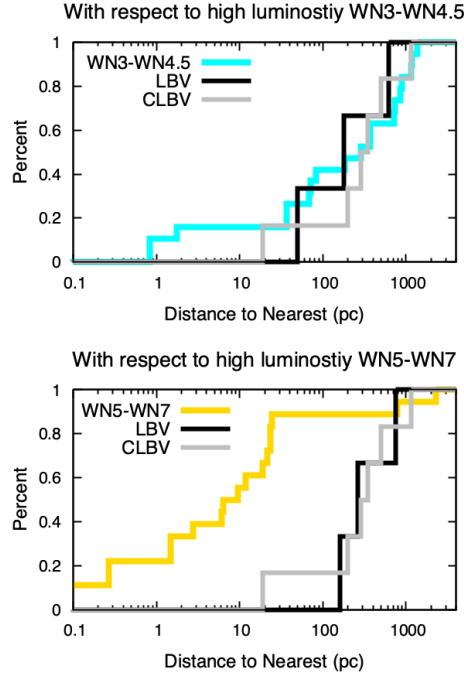


**Figure 19.** Cumulative distribution plots of the nearest neighbors for the classical LBV (black) and candidate LBV (gray) plotted relative to early (WN3-WN4.5) and late (WN5-WN7) higher luminosity ( $M_{\text{Bol}} < -9.7$ ) WN stars (colored line).

more dispersed and more isolated than the less luminous LBVs with similar luminosities. The lowest luminosity group is obviously an older subset most consistent with the A-type and yellow supergiants. Thus, based on their in-common characteristics, stars from a wide range of initial masses can display the B[e]sg phenomena along more than one evolutionary path.

The standard explanation for the WR stars is that they are OB stars which have been stripped of their hydrogen envelopes either through mass loss or binary interaction. The high luminosity earlier type WN (WN3-WN4) have a distribution similar to evolved late O-type supergiants while the later type WN's (WN5-WN7) are even less dispersed than the main sequence early O-type stars (Figure 13). This appears to call into question the expected relationship between later type WNs and LBVs. For example, two of the classic LBVs and two candidates are classified as late WN's in their quiescent states. Consequently, it was suggested that the high luminosity LBVs would eventually become late WN's. The WN spectral characteristics in the LBVs are likely due to the decrease of their H-rich envelopes through LBV mass loss episodes. The nearest neighbor analyses in Figure 19 clearly show a similar spatial distribution between classic LBV and the early-type WNs. The late WN distribution, however, confirms what we saw in Figure 13 with the strong qualification that it reflects the late WN's high concentration in the 30 Dor region. It is not surprising that the LBVs and high mass losing early WNs are correlated but it is premature to conclude that the high luminosity LBVs do not first pass through the late-WN stage, even briefly.

The late- and early-type less luminous WNs, below the H-D limit, show similar spatial distributions. Their spatial distribution map (Figure C1) shows a strong correlation with the H II regions and their nearest neighbor cumulative distributions are consistent with the late B-type supergiants, and like

the less luminous LBVs, also with more evolved A-type and yellow supergiants. The early-type less luminous WNs have presumably shed most of their H-rich envelopes, however the standard mass loss prescription for B-type supergiants from line-driven winds is not high enough in this luminosity range, and even less so with clumping, to strip their outer envelopes. In this luminosity range, mass exchange in binaries is a more plausible path from evolved B-supergiant to WN, perhaps similar to the B[e]sg. Alternatively, it is often suggested that the less luminous LBVs will eventually become WNs via their high mass loss episodes. The correlation of both groups with the more evolved supergiants as well as possible post-RSG evolution supports this outcome. We do not have sufficient data to distinguish among these possibilities, but the data at hand favor a post-LBV or post-RSG origin for the less luminous WNs.

The WC stars have a similar spatial distribution to stars which could have evolved through the yellow and red supergiant phases (Figure 15), and Figure 16 shows that the WC and less luminous WN stars have been drawn from the same population. Evolutionary tracks suggest the few WC above the HD Limit could have evolved to their present point from less luminous post-RSG progenitors. Combined with what is already established by other means, including abundance analysis, the information gleaned from the WN and the WC distributions favor the standard scenarios in which the less luminous WN and the WC stars are drawn from the same populations with the WC stars representing a more evolved state showing the products of He-burning.

Our results for the other WRs show differences and possible associations between the sub-classes of stars exhibiting the Wolf-Rayet phenomenon. “Slash” stars are most associated with very recent high mass star formation, almost all of them in a projected area 10 pc across in the heart of 30 Doradus. Both the Of/WN slash stars and high luminosity late WN are highly concentrated in the core of 30 Doradus. This may support the evolutionary link between them proposed by Crowther & Walborn (2011). However, as noted previously, the core of 30 Doradus is heterogeneous with a spread of different aged populations. Since both Of/WN slash stars and high luminosity late WN are significantly concentrated in one unique star forming region there is a potential for bias when comparing them with populations spread over different size scales in the LMC. The lower luminosity WN ( $-8.0 > M_{bol} \geq -9.7$ ), WC and WN3/O3 show indications that they are drawn from the same population reinforcing the suspected evolutionary links between them (Figures 14 and 16). The WO sample is too small to draw clear conclusions.

#### 4.1. *Transverse Velocities of LBVs and B[e]sg*

In a recent paper, Deman & Oey (2024) argue that a subgroup of LBVs, candidate LBVs, and B[e]sg in the LMC are accelerated and the products of binary mass transfer. They used the GAIA DR3 proper motion catalog to measure the transverse velocities of LBVs and B[e]sg and then compared their motions with a sample of OBe stars in the SMC. Here we show that as a class most LBVs and B[e]sgs are not associated with runaways.

Deman and Oey adopt the list of LBVs, candidates, and B[e]sgs from Agliozzo et al. (2019) with some additions and corrections. As mentioned in §2.1 that list includes two non-LBVs and two  $\alpha$

Cyg variables<sup>1</sup> They also adopt the dust-based classification from [AglioZZo et al. \(2019\)](#) which is based on the presence of or lack of mid-IR dusty emission. This classification scheme disregards the astrophysically important information from their positions on the HR Diagram; their temperatures, luminosities, possible evolutionary state, and associated stellar population.

Furthermore, many of the LBVs with dusty emission are in H II regions which also have a dusty signature. For example, R143 has a dusty nebula with an estimated dust mass of  $0.055 M_{\odot}$  or a total mass, dust plus gas, of approximately  $5.5 M_{\odot}$  ([AglioZZo et al. 2019](#)); high for an LBV. Assuming a nominal mass loss rate of  $\approx 5 \times 10^{-5} M_{\odot}$  per year during its high loss stage and it is in this state about half the time, it would take  $10^5$  years for R143 to shed that much mass. [AglioZZo et al. \(2019\)](#) acknowledge that R143 is not sufficiently luminous to ionize the nebula. Thus the dusty excess in its SED is probably associated with star formation in the H II region. Two of the CLBVs and the LBV R71 with dusty emission are not identified with H II regions. Alternatively, the dusty excess may be a residual from a prior RSG state, a possibility for the less luminous LBVs.

To calculate the relative transverse velocities for comparison, Deman and Oey selected a reference field population with Gaia magnitude  $G < 18$  within three arc minutes of the targets ( $\sim 5600 \text{ pc}^2$  at the distance of the LMC). The number of field stars compared to each target is typically more than 100 and, for many cases, several hundred stars. The brightness criteria (Gaia magnitude  $G < 18$ ) ensures this will be a very mixed population with a wide range in luminosities including stars much fainter and less massive than the LBVs and B[e]sg.

Throughout this work we have emphasized the importance of comparing these evolved stars with the population of stars that share their locus in the HRD. As the stars disperse with age we should expect the stars they are born with to be equally dispersed. Their spatial distributions and cumulative distributions in the nearest neighbor analysis confirm this. Consequently, we need to compare the motions of the target stars with similar luminosity stars. To properly analyze their motions we need to know more about the reference populations; the spectral types and luminosities in addition to the transverse velocities and errors, and the velocity spread for the field stars. Furthermore, to compare the target's velocities with models for competing ejection mechanisms requires measuring their velocities relative to their point of origin. The LMC reference field established by Deman and Oey does not appear to be consistent with that requirement.

Instead, Deman and Oey compare the LMC stars with a survey of OBe stars in the SMC ([Phillips et al. 2024](#)) which is not only a different, smaller galaxy, but a significantly different stellar population with only one confirmed LBV, R40. The full OBe sample is heavily biased towards lower mass, less luminous stars. [Phillips et al. \(2024\)](#) acknowledge that their criteria are also biased against high mass walkaway stars and note that the more massive stars in their runaway SMC OBe sample are moving faster than the average computed for the full sample. Nevertheless, Deman and Oey conclude that the LBVs and candidates in their class 1 with dusty emission and the B[e]sg have velocity distributions similar to the OBe runaways in the SMC. They comment that their second group, class 2, with no dust, does not show any evidence for acceleration. Class 2 includes the LBV HD269582, which has

<sup>1</sup>

HD 268939 (R 74), HD 269050 (R 78), HD 269128 (R 81), and HD 269445 (R 99). Interestingly, LHA 120-S 18 in their list may be a case of mistaken identity. A star labeled S 18 is included in [van Genderen \(2001\)](#) as an LBV candidate, but all of the references are to LHA 115-S 18 in the SMC, a well known B[e]sg ([Zickgraf et al. 1989](#)). LHA 120-S 18 in the LMC is an emission line star but there are few published references to its spectrum and none to variability.



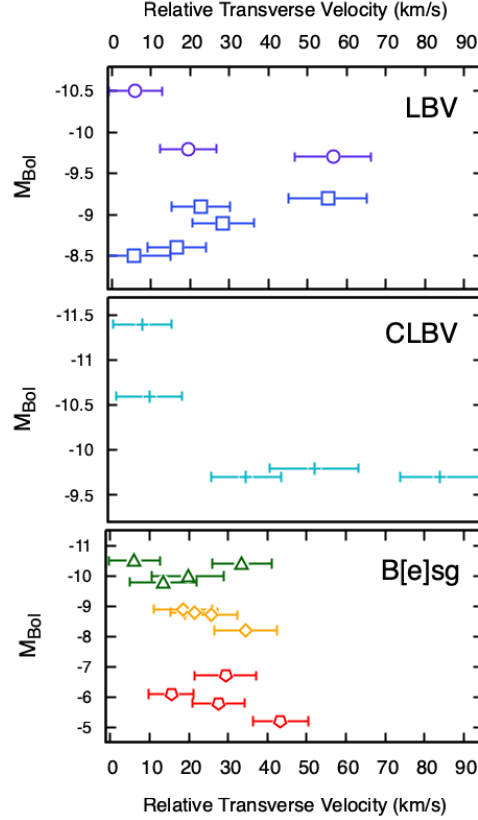


**Figure 20.** Luminosity ( $M_{Bol}$ ) as a function of relative transverse velocity (Deman & Oey 2024) with one sigma error bars for: LBVs (top panel), Candidate LBVs (middle panel) and B[e]sg (bottom panel). In the top panel: higher luminosity LBVs (purple circles,  $M_{Bol} < -9.7$ ) and less luminous LBVs (blue squares,  $M_{Bol} \geq -9.7$ ). In the bottom panel: high luminosity B[e]sg (green triangles,  $M_{Bol} < -9.7$ ), mid-luminosity B[e]sg (orange diamonds,  $-9.7 \leq M_{Bol} < -7.0$ ), and low luminosity B[e]sg (red pentagons,  $M_{Bol} \geq -7.0$ ).

a high velocity (Figure 20), and two LBV candidates, but the other four members are neither LBVs nor candidates. See the footnote 1 at the beginning of this section. Class 2 is not a realistic subset.

For these reasons, we re-examine the Deman and Oey results using the LBVs, candidates, and B[e]sgs from Tables 1 and 2 in this paper with the classification based on their positions on the HRD. Figure 20 reveals a somewhat different, more nuanced picture of the velocity distributions of the LBVs, candidate LBVs, and the B[e]sg. Their luminosities are shown relative to their transverse velocities from Table 3 in Deman & Oey (2024). Most of the confirmed LBVs have transverse velocities less than  $30 \text{ km s}^{-1}$ . The two with higher velocities between  $50$  and  $60 \text{ km s}^{-1}$  are the less luminous LBV R71 which we have previously noted is isolated compared to the stars of comparable luminosity and temperature, and the LBV HD 269582 which although not isolated has the largest separation from stars of comparable luminosity for the three classic LBVs. The candidates include two stars with high velocities; the very high velocity and apparently isolated S61 and S119 which is associated with a somewhat less luminous population mentioned in §3.1. In contrast, the B[e]sg show a relatively random distribution of velocities with luminosity, with a wide spread for each luminosity subgroup.

The velocity cutoff for candidate runaway stars suggested by Phillips et al. (2024) in their SMC OBe sample is  $24 \text{ km s}^{-1}$ . Adopting this velocity as a marker, the average relative transverse velocities for the two high luminosity classic LBVs is  $13 \text{ km s}^{-1}$ . The four less luminous LBVs with lower masses and somewhat longer lifetimes have a slightly higher average at  $18.4 \text{ km s}^{-1}$ , although one has a transverse velocity slightly above the  $24 \text{ km s}^{-1}$  cut-off. Thus the majority of the confirmed LBVs are not candidate runaway stars. The two most luminous candidate LBVs are likewise not runaway stars, although as a set, the candidates include three stars with velocities above the suggested cutoff for runaways. The B[e]sg at all luminosities, have some stars above this nominal  $24 \text{ km s}^{-1}$  with about half of the lowest luminosity set somewhat above this cutoff. These stars are older than the more luminous B[e]sg, and we consider the B[e]sg as a group to be an older population than the LBVs, and therefore more dispersed. There is no evidence from their velocities to conclude that the B[e]sg are runaways.

As another check on the interpretation of the velocities, in Figure 21 we compare the relative velocities of each star with the separation from their nearest neighbor of similar luminosity and spectral type. The nearest neighbor is *not* necessarily the point of origin, so this cannot be used to place precise limits on the ages of the individual stars. However, Figure 21 reveals an important

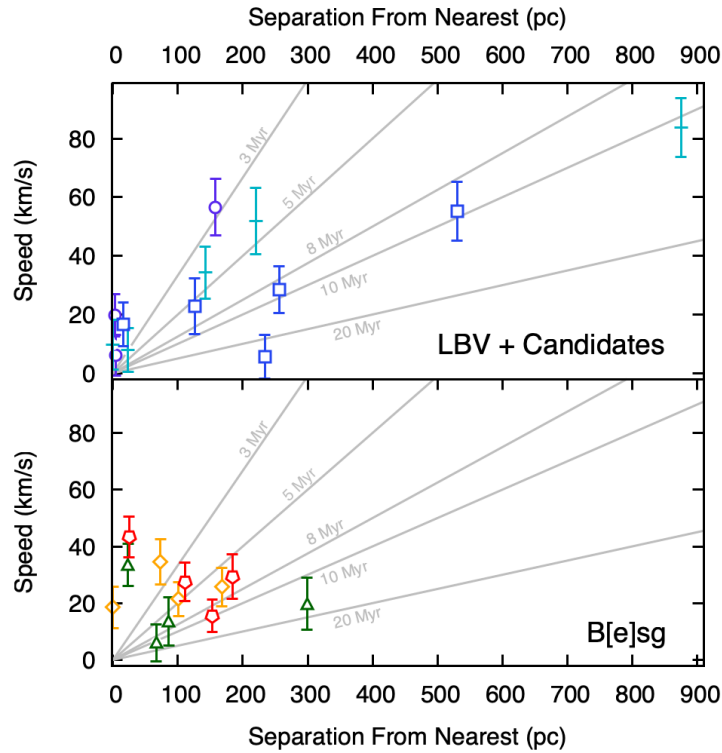


**Figure 21.** The relative transverse speed with one sigma error bars computed by Deman & Oey (2024) as a function of separation from the nearest neighbor of similar luminosity and spectral type (Tables 4 and 5). The gray lines note the distance a star will move in 3, 5, 8, 10, and 20 Myr at a given speed. The colors for each class and luminosity grouping are the same as used in Figure 20. In the top panel: higher luminosity LBV (purple circles,  $M_{Bol} < -9.7$ ), less luminous LBVs (blue squares,  $M_{Bol} \geq -9.7$ ), candidate LBV (cyan crosses). In the bottom panel: high luminosity B[e]sg (green triangles,  $M_{Bol} < -9.7$ ), mid-luminosity B[e]sg (orange diamonds,  $-9.7 \leq M_{Bol} < -7.0$ ), and low luminosity B[e]sg (red pentagons,  $M_{Bol} \geq -7.0$ ).

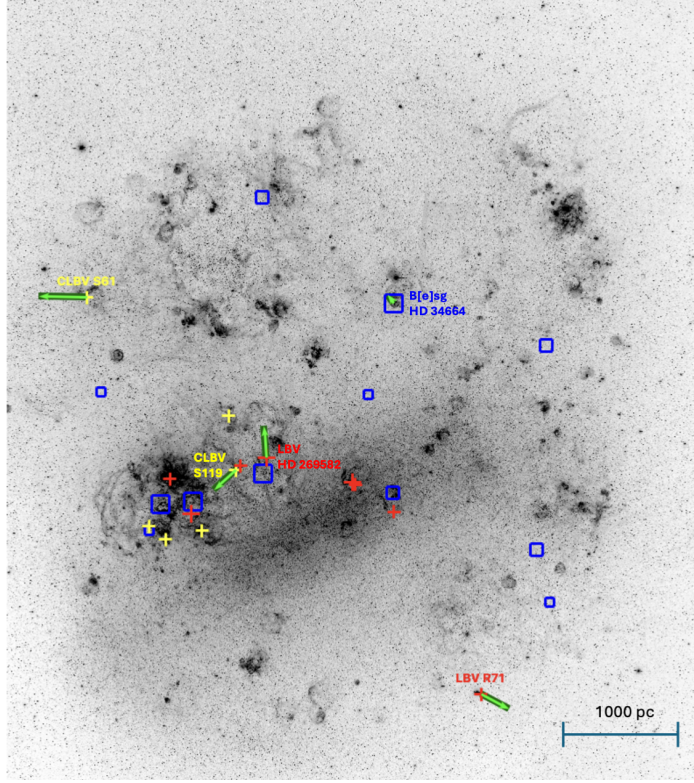


**Figure 22.** An H-alpha emission image of the LMC from MCELS (Smith & MCELS Team 1999) including LBVs (red crosses), candidate LBVs (CLBVs, smaller yellow crosses) and B[e]sg (blue boxes) in the LMC. The largest symbols for the LBV and B[e]sg are for those with  $M_{bol} < -9.7$ . Next largest symbols for those between  $-8 > M_{bol} \geq -9.7$ . And the smallest boxes for B[e]sg with  $M_{bol} > -7$ . The green arrows show the direction and amount of transverse motion that the highest velocity stars and most separated B[e]sg (labeled) will experience over 5 Myr at the relative transverse velocity that Deman & Oey (2024) has computed for them.

trend; younger populations need faster speeds to achieve larger separations. That trend is present in the LBVs and candidate-LBVs, implying they are a younger population than the B[e]sg, which have slower speeds even at larger separations. This is also supported by Figure 22 which shows that B[e]sg are widely spread across the LMC, as is expected for an older population.

LBV HD 269582 and candidate S 119 have relatively high velocities but could traverse the separations with their nearest neighbors in 3-5 Myr. Hung et al. (2021) note the nebula around S 119 appears to be in a bubble blown by the star itself with a sharper, denser edge in the direction of the star's motion. While they could be runaways, their travel times imply they could be a product of single star evolution. There is no obvious contradiction which requires rejuvenation through mass transfer as advocated by Smith & Tombleson (2015), Smith (2019), Aghakhanloo et al. (2022), and others. The high luminosity B[e]sg, HD 34664, has a greater separation from similar stars than the other B[e]sgs, and may have received some additional acceleration from binary interaction since binarity is a possible explanation for these stars' properties.

LBV R71, lying below the 8 Myr line in Figure 21, is clearly the exception among LBVs. It has a separation of 530 pc from its nearest neighbor of similar type which would take almost 10 Gyr

to traverse at  $55 \pm 10 \text{ km s}^{-1}$ . This would be hard to explain at its luminosity even as a post-RSG. [Lennon et al. \(2017\)](#) also noted that R71 is "rather unique in its isolation" with an apparent discrepancy between its probable age and time to travel from a group of OB stars (see Figure B2) 450 pc to the north of R71.

Candidate S61 is similar. Its high velocity ( $83.8 \text{ km s}^{-1}$ ) and isolation compared to the other candidates, suggests it may be a runaway. While it is isolated from other high luminosity stars, there are three less luminous ( $M_{\text{Bol}} > -9.7$ ) WN and six less luminous OB stars within 100 pc. It is also associated with loose filamentary H II emission DEM L 308 / [KDS99] SGS 94 ([Davies et al. 1976](#); [Kim et al. 1999](#)). [Hung et al. \(2021\)](#) classified the nebula as a "large structure (i.e. super bubble)" about 85 pc across with an expansion age between 2-4 Myr embedded in an H I shell. While there is an ionizing association of OB stars on its rim to the northwest, this structure may be a supernova remnant. The origin of S61's high velocity may be associated with this expanding nebula.

Among the LBVs and candidates, R71 and S61 are the only two that may require additional acceleration. Both dynamic ejection and the binary supernova scenario however, do not inevitably result in significant mass gain. In fact, abundance analysis of runaway OB stars in the solar neighborhood, including those likely to have been accelerated by the binary supernova scenario, show *no* evidence of processed material transferred onto their surfaces ([Martin 2006](#); [McEvoy et al. 2017](#); [Liu et al. 2023](#)).

## 5. CONCLUSIONS

The following summarizes our conclusions.

- The majority of LBV/S Dor variables and candidates are not isolated from stars of similar luminosity and spectral type. The majority of confirmed LBVs are not runaways.
- LBV R71 and candidate S61 have high velocities that require acceleration.
- The nearest neighbor discussion of the B[e]sg is consistent with stars of the same spectral type and luminosity range although their spatial distribution and velocity spread suggests that they are an older population than the LBVs.
- The early-type high luminosity WNs are correlated with the late O-type stars and with the most luminous LBVs. Conclusions about the late WNs are limited by their high concentration in the 30 Dor region.
- The less luminous WNs, and WCs are most closely associated with more evolved stars in the  $20 - 40 M_{\odot}$  range including late-type B, A-type supergiants and yellow hypergiants.
- The less luminous WNs, WN3/O3, and WC stars have similar spatial distributions, suggesting association with each other and a possible evolutionary link.
- The nearest neighbor results for the less luminous LBVs, less luminous WNs and WCs are consistent with a post-yellow hypergiant origin.

Martin's contribution to this work is supported by the Henry R. Barber Astronomy Observatory Endowment at the University of Illinois Springfield. We thank P.A. Crowther for his feedback on the census of the most luminous stars in the 30 Dor presented in our previous paper.

## APPENDIX

### A. UPDATES TO THE CATALOG OF LUMINOUS STARS IN THE LMC

Twenty (25) stars from Walborn et al. (1999), 12 stars from Walborn et al. (2010), 6 stars from Bestenlehner et al. (2014), and 21 stars from Castro et al. (2021) with good spectral types and photometry have been added to the list OB-type supergiants (Table A1) and OB-type known and suspected binaries (Table A2). When available, luminosity and effective temperatures from Walborn et al. (2014a) were adopted. Otherwise physical parameters are derived from their spectral type according to the procedure in Martin & Humphreys (2023).

The intrinsic colors and bolometric corrections for O2 – O3.5 types were revised according to Doran et al. (2013) and Sabín-Sanjulián et al. (2017) (Table A4). Updated parameters for the earliest O-type supergiants are given in Table A1.

Twenty (20) stars were duplicated between the O- and B-type supergiant lists. Each was classified by (Rousseau et al. 1978) as an early B-type without luminosity class then re-classified by a subsequent survey as a later O-type with luminosity class. In Martin & Humphreys (2023) we gave preference to the spectral types with luminosity class over the classifications of Rousseau et al. (1978). The following stars have been removed from the B-type supergiant list but remain in the O-type supergiants list: SK -67 4, SK -70 13, SK -69 29, SK -66 47, SK -70 57, SK -70 66, SK -70 70, HD 269244, SV\* HV 2543, SK -67 150, HD 271363, HD 271366, SK -67 250, SK -68 166, SK -70 117, SK -68 180, SK -67 118, HD 269215, SK -67 119, and BI 137.

The VFTS survey of the 30 Doradus region focused primarily on luminous early type stars but the initial sample for that survey was magnitude limited and included a number of late type stars (see Table 3 in Evans et al. (2011)). Combining information from that survey with McGregor & Hyland (1981), Davies et al. (2018), and Britavskiy et al. (2019) six (6) stars were added to the RSG sample and one star was added to the A-type supergiants (Table A3).

The star SK -70 13 / LB 3400 was listed twice in the B-supergiant list. They appear to be the same star so the entry for LB 3400 was removed.

The star CPD -69 448 is misclassified in the Simbad database and Martin & Humphreys (2023). Simbad cites Evans et al. (2015) as the source of the spectral type but CPD -69 448 = VFTS 271 is not typed in that publication. Melnick (1985) classifies it as A Ib and Evans et al. (2011) assigns it A7 II. CPD -69 448 was moved from the B-type star list into the A-supergiant list. The re-calculated parameters for it are given in Table A3.

### B. MAPS OF LUMINOUS STARS IN THE LMC

In Figures B1 – B5, the reference samples (Table 3) are plotted on maps of H-alpha emission from the UM/CTIO Magellanic Cloud Emission-line Survey (MCELS) (Smith & MCELS Team 1999).



Table A1. Additional OB-Type Supergiants

RAJ2000	DecJ2000	Name	V	(B-V)	(U-B)	Phot		SpType		Log( $T_{eff}$ )	$M_{Bol}$
						Source <sup>a</sup>	SpType	Source <sup>a</sup>	$A_V$ <sup>b</sup>		
72.36675	-67.71119	SK -67 3	13.18	-0.23	-1.11	Z04	O7.5nfp	M17	0.18	4.54	-8.98
72.79409	-69.55573	[MNM2015] LMC156-2	13.65	-0.13	-1.15	Z04	O6.5 Ifp	M17	0.57	4.56	-8.81
74.14046	-66.47367	PGMW 1180	12.99	-0.17	-1.10	W99	O8.5II(f)	W99	0.35	4.51	-8.97
74.14213	-66.47381	PGMW 1191	14.90	-0.19	-1.02	W99	O9.5V	W99	0.25	4.50	-6.89
74.14313	-66.47439	Sch95 8	14.87	-0.28	-0.99	W99	O8.5V	W99	0.01	4.53	-6.86
74.14313	-66.47503	PGMW 1197	15.04	-0.24	-0.91	W99	B0V	W99	0.03	4.49	-6.46
74.14354	-66.47436	PGMW 1199	13.57	-0.21	-0.99	W99	O7.5III	W99	0.25	4.54	-8.66
74.14371	-66.47392	Sch95 6	14.77	-0.24	-0.96	W99	O9.5V	W99	0.09	4.50	-6.86
74.14417	-66.47378	Sch95 7	14.91	-0.27	-1.03	W99	O9V	W99	0.03	4.52	-6.75
74.14467	-66.47381	Sch95 1	12.56	-0.18	-1.01	W99	O9Ib	W99	0.31	4.50	-9.24
74.14475	-66.47408	Sch95 5	14.74	-0.23	-1.00	W99	O9.5V	W99	0.12	4.50	-6.92
74.14517	-66.47464	PGMW 1212	14.66	-0.26	-0.95	W99	O8V	W99	0.08	4.54	-7.22
74.14525	-66.47314	PGMW 1213	13.82	-0.26	-0.99	W99	O8V((f))	W99	0.08	4.54	-8.06
74.31329	-69.33900	SK -69 50	13.37	-0.16	-1.04	Z04	O7(n)(f)(p)	W10a	0.40	4.56	-8.93
74.68703	-66.20405	SK -66 44	13.12	-0.30	-0.90	Z04	O6.5(n)fp	W10a	0.04	4.58	-8.97
79.70625	-69.25167	2dFL51-106	12.84	-0.14	-	U00	O7(n)fp	W10a	0.46	4.54	-9.44
80.22792	-65.45500	SK -65 47	12.47	-0.20	-0.87	Z04	O4I(n)f+p	W10a	0.42	4.61	-10.19
82.25712	-68.53436	SK -68 96	13.26	-0.15	-1.08	Z04	O7Ianf	W10a	0.43	4.54	-8.98
82.78383	-68.61508	SK -68 112	12.82	-0.18	-	Z04	O7.5(n)(f)(p)	W10a	0.33	4.53	-9.27
82.96708	-67.57250	HD 269702	11.99	-0.30	-	H00	O8I(f)p	W10a	0.00	4.52	-9.67
83.38057	-67.48273	[MNM2015] LMCe136-2	14.69	-0.16	-1.15	Z04	O6nfp	N18	0.47	4.59	-7.90
83.99421	-69.19775	H-M 6	14.14	0.04	-0.92	Z04	O8V	W99	1.01	4.54	-8.67
83.99867	-69.19704	H-M 8	14.30	0.01	-0.88	W99	O8III	W99	0.91	4.53	-8.34
83.99896	-69.19793	H-M 11A	15.15	0.09	-0.74	W99	O7.5V	W99	1.17	4.55	-7.91
83.99904	-69.19733	H-M 7	14.01	0.01	-1.03	W99	O4III	W99	1.05	4.63	-9.42
84.01892	-69.19725	H-M 9A	13.42	-	-	W99	O4If+	W99	0.00	4.61	-10.00
84.02667	-69.19667	SK -69 212	12.42	-0.02	-	Z04	O5n(f)p	W10a	0.95	4.59	-10.64
84.36637	-69.39789	UCAC4 104-015116	13.38	-0.16	-1.08	Z04	O5nfp	M17	0.49	4.61	-9.38
84.44258	-69.15283	Testor 1998 1B	15.10	0.20	-1.00	W99	O7V	W99	1.52	4.57	-8.39
84.44267	-69.15317	Testor 1998 1C	15.40	0.03	-0.58	W99	B1-2	W99	0.64	4.30	-5.63
84.44392	-69.15230	Testor 1998 2B	15.19	0.18	-1.23	W99	O8III	W99	1.44	4.53	-7.98
84.44417	-69.15222	[TLD88] 2A	14.13	0.13	-	W99	O4(n)(f)p	W99	1.43	4.61	-9.54
84.63750	-69.08700	Cl* NGC 2070 SMB 131	15.26	-0.06	-0.80	VFTS,P93a	O9.5(n)	W14	0.65	4.50	-6.93
84.66370	-69.11090	Cl* NGC 2070 SMB 365	16.38	0.54	-0.37	VFTS,Z04	O5:Vn	H12	2.67	4.61	-8.56
84.67010	-69.10130	Cl* NGC 2070 MH 95	15.38	0.39	-	VFTS	O9.5III/V	H12	2.05	4.50	-8.21
84.67120	-69.10050	Cl* NGC 2070 MH 129	14.68	0.17	-	VFTS	O6.5III/V	H12	1.46	4.58	-8.80
84.67180	-69.09780	[P93] 841	15.53	0.17	-1.10	P93a	O4-6(n) (f)p	W10a	1.52	4.61	-8.61
84.67520	-69.10470	Cl* NGC 2070 MH 314	15.51	0.15	-	VFTS	O3-4	H12	1.49	4.63	-8.50
84.67680	-69.10180	Cl* NGC 2070 MH 623	15.20	0.30	-	VFTS	O8.5III/V	H12	1.81	4.52	-8.19
84.67780	-69.10310	Cl* NGC 2070 MH 591	15.26	0.14	-	VFTS	O8III/V	H12	1.36	4.54	-7.63
84.67860	-69.08750	[P93] 994	15.54	0.01	-0.86	P93a	B0:V	SIM	0.83	4.49	-6.61
84.68030	-69.10459	Cl* NGC 2070 MH 749	13.80	0.04	-	VFTS	O3 III(f*) or O4-5V	W14	1.02	4.67	-10.04
84.68160	-69.09150	Cl* NGC 2070 SMB 240	16.13	-0.02	-1.04	VFTS,Z04	B0-0.5V	E15b	0.74	4.49	-5.84
84.68400	-69.09910	Cl* NGC 2070 MH 859	13.76	0.12	-0.62	P93a	O3III(f+)	M05a	1.40	4.67	-10.35
84.68430	-69.09640	Cl* NGC 2070 MH 878	13.36	1.70	-	VFTS	O8II	SIM	1.27	4.53	-9.57
84.69080	-69.09470	[CHH92] 7012	14.73	0.12	-1.04	P93a	O7	SIM	1.27	4.57	-8.43
84.69520	-69.10740	Cl* NGC 2070 SMB 408	16.73	0.17	-2.47	VFTS,Z04	B0vn	E15b	1.34	4.49	-5.84
84.71570	-69.10040	Cl* NGC 2070 SMB 229	15.96	0.04	-0.67	VFTS,Z04	B0-0.5V(n)	E15b	0.86	4.45	-5.92

<sup>a</sup> E15a = Evans et al. (2015), H00 = Høg et al. (2000), H12 = Hénault-Brunet et al. (2012), M05a = Massey et al. (2005), M17 = Massey et al. (2017), N18 = Neugent et al. (2018), P93a = Parker & Garmany (1993), SIM = classification given in SIMBAD which Wenger et al. (2000) identify as either from Houk & Cowley (1975) or Jaschek (1978), VFTS = Evans et al. (2011), U00 = Udalski et al. (2000), W10a = Walborn et al. (2010), W14 = Walborn et al. (2014b), W99 = Walborn et al. (1999), Z04 = Zaritsky et al. (2004).

<sup>b</sup> Extinction estimated from spectral type.



**Table A3.** Additional Late-Type Supergiants in 30 Doradus

RAJ2000	DecJ2000	Name	$J^a$	$H^a$	$K_s^a$	$V^b$	$(B-V)^b$	SpType	$A_V^f$	$\text{Log}(T_{eff})^d$	$M_{Bol}^f$
Red Supergiants											
84.566667	-69.16983056	V* Z Dor	9.308	8.336	7.867	14.22	2.28	M4 Ia-Ib <sup>3</sup>	0.71	3.55	-7.60
84.569500	-69.07058056	2MASS J05381667-6904140	9.786	8.906	8.552	13.99	2.40	M <sup>4</sup>	0.50	3.57	-7.08
84.611208	-69.14797222	WHO S 452	9.782	8.754	8.34	14.02	2.46	K5 Ia-Ib <sup>3</sup>	0.66	3.57	-7.25
84.701917	-69.09241389	W61 7-8	9.173	8.297	7.86	13.62 <sup>2</sup>	2.31 <sup>2</sup>	M3.5 Ia <sup>3</sup>	0.63	3.57 <sup>e</sup>	-7.75
84.914208	-69.19779167	W61 8-4	9.864	8.965	8.524	14.52	2.20	Early M <sup>5</sup>	2.50 <sup>6</sup>	3.59	-7.58 <sup>6</sup>
84.924083	-69.19194722	W61 8-7	10.28	9.352	8.935	14.64	2.16	M <sup>4</sup>	0.63	3.60	-7.75
A-type Supergiants											
84.564040	-69.0675800	CPD-69 448	10.865	10.279	10.06	12.24	0.21	A7 II <sup>5</sup>	0.27 <sup>e</sup>	3.92 <sup>e</sup>	-6.51 <sup>e</sup>
84.908000	-69.19613611	VFTS 820	10.865	10.279	10.06	12.73 <sup>1</sup>	0.55 <sup>1</sup>	A0 Ia <sup>5</sup>	1.70 <sup>e</sup>	3.98 <sup>e</sup>	-7.51 <sup>e</sup>

<sup>a</sup> From 2MASS point source catalog (Cutri et al. 2003).

<sup>b</sup> From the VFTS catalog (Evans et al. 2011) unless otherwise noted.

<sup>d</sup> Estimated by Britavskiy et al. (2019) unless otherwise noted.

<sup>e</sup> Estimated using the method outlined in Martin & Humphreys (2023)

<sup>f</sup> Estimated by Davies et al. (2018) unless otherwise noted.

<sup>1</sup> Massey (2002)

<sup>2</sup> Parker (1993)

<sup>3</sup> González-Fernández et al. (2015)

<sup>4</sup> McGregor & Hyland (1981)

<sup>5</sup> Evans et al. (2011)

<sup>6</sup> Britavskiy et al. (2019)

**Table A4.** Adopted Values by Spectral Type

Sp. Type	<i>Supergiants (I)</i>			<i>Giants (III)</i>		<i>Dwarfs (V)</i>	
	$(B-V)_0$	$\text{Log}(T_{eff})$	B.C (mags)	$\text{Log}(T_{eff})$	B.C (mags)	$\text{Log}(T_{eff})$	B.C (mags)
O2	-	-	-	4.695	-4.34	4.727	-4.58
O3	-0.33	4.626	-3.87	4.672	-4.20	4.663	-4.12
O4	-0.33	4.607	-3.74	4.628	-3.88	4.632	-3.91

**Table A2.** Additional OBA-Type Known and Suspected Binaries

RAJ2000	DecJ2000	Name	V	(B-V)	(U-B)	Phot	Binary	SpType	$a_V$	$b_V$	$\text{Log}(T_{eff})$	$M_{Bol}$
74.14054	-66.47328	PGMW 1181	14.19	-0.24	-0.99	W99	SB	O9Vn(sb?)	W99	0.124	4.52	-7.56
74.142047	-66.47383	OGLE LMC-ECL-27754	15.08	-0.28	-0.83	W99	SB	B1V	W99	0.213	4.36	-6.60
74.14354	-66.47411	PGMW 1198	14.88	-0.27	-0.92	W99	Blend	B0.5-B1V	W99	0.213	4.39	-6.17
84.44200	-69.15246	VFTS 145	14.30	0.19	-	VFTS	SB	O8fp	W14	1.49	4.52	-9.36
84.44338	-69.15338	IRSF J05374638-6909120	15.30	0.12	-0.11	W99	SB	O9.5V	W99	1.209	4.50	-7.45
84.44463	-69.15313	IRSF J05374670-6909112	15.30	0.06	-1.06	W99	Blend	O7V	W99	1.085	4.57	-7.76
84.66250	-69.11640	Cl* NGC 2070 SMB 278	15.86	0.44	0.63	VFTS,M02	SB	O7.5V+O7.5V	W14	2.26	4.55	-8.15
84.66540	-69.10240	[P93] 729	15.26	0.10	-1.07	VFTS,P93a	Blend	O6-7dbl	H12	1.24	4.58	-8.00
84.67120	-69.08700	Cl* NGC 2070 SMB 81	14.66	-0.06	-	VFTS	Blend	O3.5V((f))z+OB	W14	0.84	4.64	-8.73
84.67298	-69.11383	Cl* NGC 2070 MH 203	13.67	0.61	-	VFTS	Blend	O3 V + mid/late O	W14	2.91	4.66	-10.82
84.67390	-69.10530	Cl* NGC 2070 SMB 154	16.55	0.17	-2.14	VFTS,Z04	SB	O8.5 V	W14	1.72	4.53	-7.16
84.67446	-69.10346	Cl* NGC 2070 MH 290	14.34	0.28	-	VFTS	Blend	O3 III(f*) + mid/late O	W14	1.77	4.63	-9.33
84.67528	-69.10394	Cl* NGC 2070 SMB 25	13.31	0.21	-	VFTS	Blend	O4 If+	W14	1.67	4.61	-11.04
84.67917	-69.07042	MH 12	13.96	-0.03	-2.32	VFTS,M02	SB	ON9Ia:+O7.5I:(f):	W14	0.78	4.50	-8.79
84.68480	-69.09850	Cl* NGC 2070 MH 887	13.55	1.70	-0.79	P93a	SB	OC2.5If*+O4V	B22	1.55	4.63	-10.43
84.68560	-69.09480	Cl* NGC 2070 MH 917	17.10	0.18	-	VFTS	SB	O9.5III-III(n)	W14	1.40	4.49	-5.92

<sup>a</sup> B22= [Bestenlehner et al. \(2022\)](#), H12 = [Hénault-Brunet et al. \(2012\)](#), M02 = [Massey \(2002\)](#), P93a = [Parker & Garmany \(1993\)](#), VFTS = [Evans et al. \(2011\)](#), W14 = [Walborn et al. \(2014b\)](#), W99 = [Walborn et al. \(1999\)](#), Z04 = [Zaritsky et al. \(2004\)](#).

<sup>b</sup> Estimated from spectral type

<sup>c</sup> Multiplicity types: Blend = unresolved blend of more than one star, SB = Spectroscopic Binary

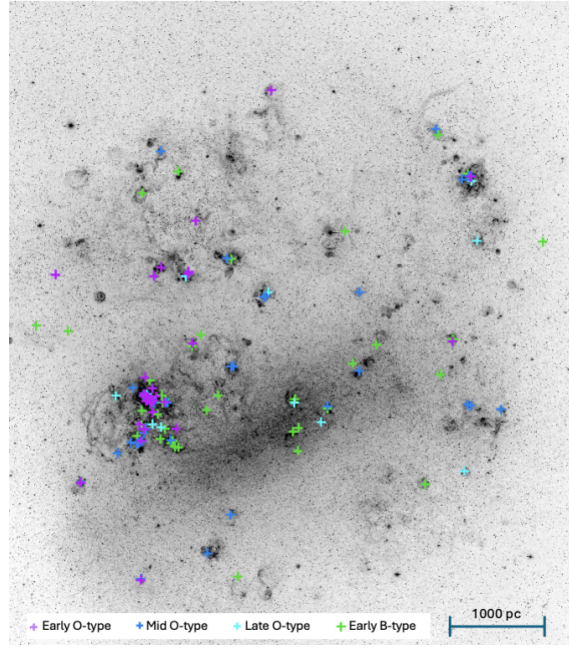


**Figure B1.** An H-alpha emission image of the LMC from MCELS (Smith & MCELS Team 1999) for the high luminosity reference samples with  $M_{Bol} < -9.7$  (Table 3): Early O-types (purple), Mid O-types (blue), Late O-types (cyan), and Early B-types (green).

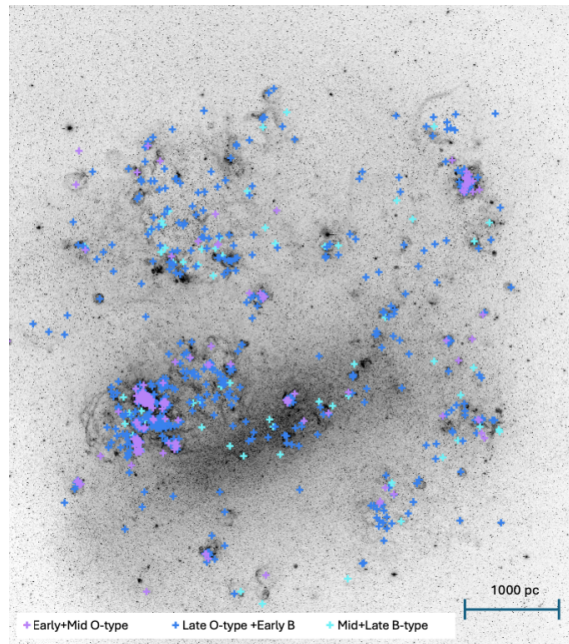


**Figure B2.** An H-alpha emission image of the LMC from MCELS (Smith & MCELS Team 1999) including the reference samples of the earliest types for  $-8 > M_{Bol} \geq -9.7$  (Table 3): Early + Mid O-types (purple), Late O-types + Early B-types (blue), and Mid + Late B-types (cyan).

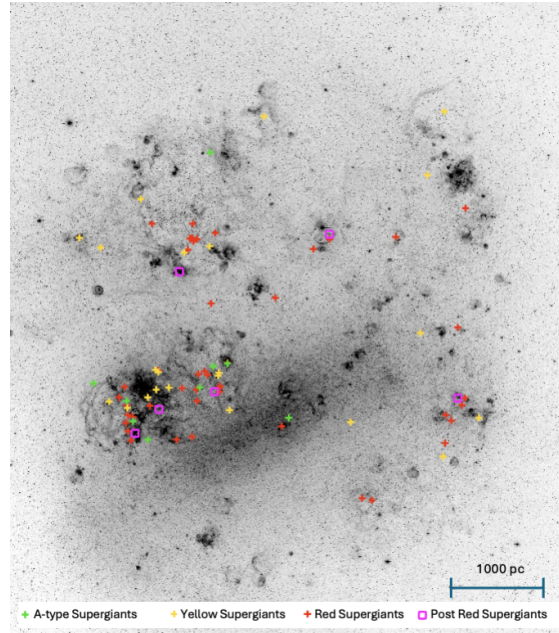


**Figure B3.** An H-alpha emission image of the LMC from MCELS (Smith & MCELS Team 1999) including the reference samples of the late types for  $-8 > M_{Bol} \geq -9.7$  (Table 3): A-type supergiants (green), Yellow supergiants (gold), Red supergiants (red) and post-Red supergiants (magenta squares).

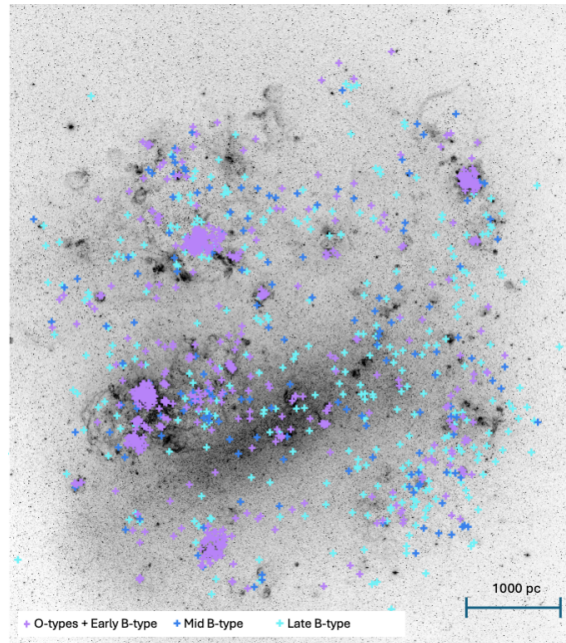


**Figure B4.** An H-alpha emission image of the LMC from MCELS (Smith & MCELS Team 1999) including the reference samples for  $-5.0 > M_{Bol} \geq -7.0$  (Table 3): O-types + Early B-types (purple), Mid B-types (blue), and Late B-types (cyan).

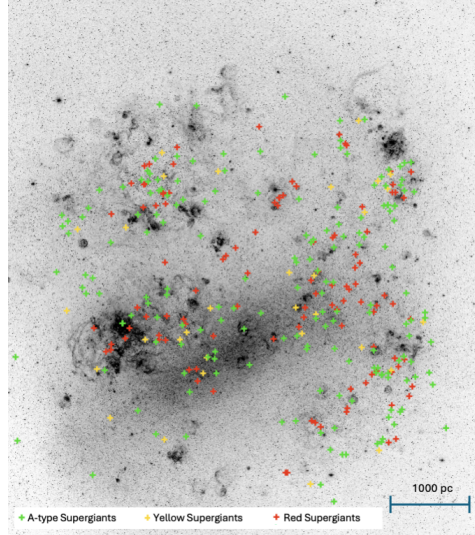


**Figure B5.** An H-alpha emission image of the LMC from MCELS (Smith & MCELS Team 1999) including the reference samples of the late types for  $-5 > M_{Bol} \geq -7.0$  (Table 3): A-type supergiants (green), Yellow supergiants (gold), and Red supergiants (red).

### C. WOLF-RAYET STARS SAMPLES

The list of WR in the LMC is taken from Neugent et al. (2018). The WN are split into higher and lower luminosity, above and below the Humphreys-Davidson limit ( $M_{Bol} = -9.7$ ).  $M_{Bol}$  values for most of the WR are given in Hainich et al. (2014). Five WN have no  $M_{Bol}$  determined by Hainich et al. (2014). [M2002]LMC 57799, [M2002]LMC 169271, and [MNM2014]LMC143-1 are all WN3 stars discussed by Massey et al. (2014). Comparing their  $M_V$  to other WN3 with known  $M_{Bol}$ , [M2002]LMC 57799 and [M2002]LMC 169271 are classified lower-luminosity and [MNM2014]LMC143-1 is classified high-luminosity. Brey 3a and LHA 120-S 131 are classified lower-luminosity based on analyses by (Moffat 1991) and (Massey et al. 2015) respectively. See Table C1.

Fifteen (15) of the 23 WC stars do not have  $M_{Bol}$  determined by previous work. The rest range between  $-8.9 \geq M_{Bol} \geq -9.9$ . The absolute visual magnitude  $M_V$  was estimated for 18 of the WC using the observed V magnitude and visual extinction ( $A_v$ ) determined by Crowther et al. (2023). Eight out of eleven brightest stars with  $M_V < -5.9$  have composite spectra indicating unresolved companions may be contributing to their brightness. The 13 WC stars without composite spectra range from  $-4.67 \geq M_V \geq -6.04$ . WC in the LMC all have the same sub type, a similar metallicity (Smith et al. 1990) and cover a relatively narrow range of brightness when accounting for unresolved companions. So they are kept together as a single sample.

The WO, WN3/O3 and Of/WN samples are also *not* split by luminosity. The WO and WC stars share a suspected evolutionary link (Aadland et al. 2022) but all 3 of the WO stars are lower luminosity (Table C2). WN3/O3 are a sub-class of WN3 and WN4 with some hydrogen in their spectra (Neugent et al. 2017). Not to be confused with the Of/WN "slash" stars, the WN3/O3 are all lower luminosity with  $M_{Bol} \geq -9.8$  (Table C1). Slash-stars (Of/WN) are a classification created by Crowther & Walborn (2011) to describe high-luminosity ( $M_{Bol} \leq -9.7$ ) stars that show a combination of Of and WN features in their spectra (Table C3).

Figures C1 and C2 show the distributions of the WR samples plotted on a map of the LMC.



**Table C1.** Wolf-Rayet WN and WN3/O3 in the LMC

RAJ2000	DecJ2000	Name	SpType	Log( $T_{eff}$ )	$M_{Bol}$	Source <sup>a</sup>
WN ( $M_{Bol} < -9.7$ )						
73.8806250	-67.5007500	HD 32109	WN3pec	5.20	-9.80	1
74.7363333	-68.8030556	HD 268856	WN4+OB	4.83	-9.85	1
77.4184167	-68.8902222	HD 34169	WN3+OB	4.70	-10.55	1
78.4323750	-67.3748333	HD 34632	WN4+OB	4.83	-10.95	1
79.5800417	-69.1946389	HD 269333	BI+WN4	4.85	-13.45	1
80.5938750	-71.5994722	HD 36063	WN6h	4.67	-10.05	1
81.6888333	-68.8313333	HD 269546	B3I+WN5	4.85	-15.20	1
81.9070000	-70.6015000	Brey 37	WN3+OB	4.83	-9.83	1
82.3883750	-70.9930278	Brey 40a	WN3+O7.5	4.85	-11.05	1
83.2940417	-67.7119722	Brey 48	WN3+OB	4.85	-11.33	1
83.6503333	-69.7601389	Sk-69 194	B0I+WN3	-	-10.50	2
83.7474167	-69.7350833	Brey 53	WN3+O	4.85	-10.33	1
83.8688333	-69.6691389	[MNM2014]LMC143-1	WN3+O8-9III	-	high	
83.9257917	-69.2095833	Brey 56	WN5h	4.67	-10.10	1
83.9345000	-68.9935556	Brey 60	WN3+abs	4.80	-10.15	1
83.9952917	-69.1966111	Brey 65	WN7	4.65	-12.18	1
83.9992500	-69.1895278	Brey 57	WN7	4.62	-10.63	1
83.9995417	-69.1973889	BAT99 80	WN5 g	4.65	-11.20	1
84.4543333	-69.0856389	HD 269891	B1I+WN3	4.65	-12.58	1
84.6400833	-69.0806944	HD 269919	WN7	4.62	-10.20	1
84.6517500	-69.1159444	Brey 81	WN7	4.67	-11.08	1
84.6631250	-69.1058889	Brey 79	WN6	4.65	-11.95	1
84.6689625	-69.0991944	Brey 75	WN6h	4.67	-10.58	1
84.6733333	-69.0872222	RMC140a	WN6	4.65	-12.20	1
84.6734167	-69.0875278	RMC140b	WN5(h)+O	4.67	-10.35	1
84.6763875	-69.1009167	BAT99 106	WN4.5h	4.75	-10.98	1
84.6766250	-69.1008056	BAT99 108	WN5h	4.75	-12.38	1
84.6767167	-69.1007778	BAT99 109	WN5h	4.75	-10.83	1
84.6787750	-69.1013333	BAT99 112	WN4.5h	4.75	-11.40	1
84.6844042	-69.1016111	Brey 84	WN4.5h	4.80	-12.83	1
84.6980000	-69.0070278	HD 269926	WN4.5	4.80	-11.20	1
84.7224167	-69.0335833	HD 38282	WN5/6+WN6/7 i	4.67	-11.85	1
84.7313750	-69.0740833	VFTS682	WN5h	4.72	-11.45	3
84.7377917	-69.1015833	HD 269928	WN6+O3.5If*/WN7	4.67	-11.63	1
84.7972083	-69.0337778	HD 38344	WN5h	4.70	-10.78	1
85.0314583	-69.4088611	HD 38472	WN3+O7	4.85	-11.30	1
85.0555417	-69.3795833	HD 38489	B[e]+WN?	4.41	-9.98	4
85.4523750	-70.5918889	Brey 97	WN3+O5V	4.90	-10.70	1
WN ( $-9.7 \leq M_{Bol} < -8$ )						
71.3843750	-70.2530278	Brey 1	WN3	4.95	-8.45	1
72.4010417	-69.3485556	Brey 2	WN2	5.15	-8.63	1
73.2391250	-66.6870833	Brey 3	WN3	4.90	-8.98	1
73.2656667	-69.3977222	[M2002]LMC 15666	WN3+O6V	4.95	-8.83	5
73.3753333	-69.2970556	Brey 3a	WNL/Of?	-	low	
73.6170833	-69.2141389	Brey 4	WN2	5.15	-8.83	1
73.7816667	-69.2088056	[M2002]LMC 23417	WN3	-	-8.80	6
74.4210000	-66.5451667	LHA 120-S 9	WN10	4.85	-9.10	1
74.9647917	-67.9487222	HD 268847	WN3	4.95	-9.13	1
75.7468333	-69.2339722	[M2002]LMC 57799	WN3+abs	-	low	
75.7871250	-66.6826389	Brey 13	WN7h	4.70	-9.70	1
76.0513750	-70.0653889	Brey 14	WN4	4.83	-9.43	1

**Table C1** continued on next page



Table C1 (*continued*)

RAJ2000	DecJ2000	Name	SpType	Log( $T_{eff}$ )	$M_{Bol}$	Source <sup>a</sup>
76.2851250	-70.3791944	Brey 15	WN3h	4.85	-9.28	1
78.4761250	-69.5296389	Brey 18	WN9	4.51	-9.58	1
78.4833750	-67.4101667	BAT99 23	WN3	4.85	-9.08	1
78.5528750	-69.3239444	Brey 19	WN3	5.00	-9.05	1
78.7386250	-71.6050833	Brey 19a	WN4ha	4.83	-9.08	1
79.1618333	-69.2780278	Brey 20	WN4	4.85	-9.25	1
80.1863750	-65.4723611	Brey 23	WN3+OB	4.85	-8.95	1
80.4904167	-65.8167500	Brey 24	WN6h	4.67	-9.33	1
80.5183750	-67.9852222	Brey 25	WN3	4.88	-8.53	1
80.8250417	-65.9491667	Brey 27	WN3	4.85	-9.20	1
81.1007917	-68.5265556	Brey 29	WN3/WCE+OB	4.85	-9.48	1
81.2264167	-66.2364167	Brey 30	WN3	4.90	-9.33	1
81.6535833	-68.8503611	Brey 33	WN4	4.45	-9.25	1
81.6774167	-69.1159444	HD 269549	WN4	5.00	-9.20	1
81.9278750	-69.1667778	Brey 36	WN7h	4.65	-9.35	1
82.0745833	-69.0433056	Brey 38	WN4	4.80	-8.80	1
82.3015417	-68.7600278	HD 269618	WN3	4.95	-9.18	1
82.3818333	-68.9080000	HD 269624	WN3	4.95	-8.70	1
82.4735000	-69.0180000	Brey 41	WN5h	4.81	-9.33	1
82.5102500	-68.7551111	Brey 42	WN3	4.95	-8.45	1
82.8252083	-69.1459722	Brey 44a	WN9	4.58	-9.58	1
82.8931667	-67.2748056	Brey 45	WN3	4.90	-8.70	1
83.0312083	-68.4421111	Brey 47	WN7h	4.67	-9.30	1
83.2952917	-69.4836111	Brey 49	WN3+OB	4.80	-9.65	1
83.6561250	-66.2438889	Brey 51	WN3	4.85	-8.73	1
83.7167917	-67.3580556	Brey 52	WN4h	4.80	-9.15	1
83.8132500	-69.0953056	Brey 55	WN3	4.83	-9.58	1
83.8741667	-67.1137222	Brey 54	WN3(h)	4.95	-9.65	1
83.9376250	-68.9790000	Brey 61	WN4+abs	4.85	-9.70	1
83.9610417	-68.8942222	Brey 63	WN5	4.78	-9.50	1
83.9684583	-68.9190833	Brey 63a	WN3+abs	4.90	-9.43	1
83.9751250	-67.0469167	Brey 59	WN4	4.85	-9.10	1
83.9765417	-68.9855278	LHA 120-S 125	WN9	4.54	-9.35	1
83.9965000	-69.1974167	Brey 65b	WN4	4.85	-9.45	1
84.0505417	-67.5827222	Brey 65a	WN5h	4.67	-8.90	1
84.1399167	-69.1548056	Brey 66	WN3	5.00	-9.03	1
84.2978333	-69.1272778	Brey 69	WN3	4.95	-8.53	1
84.3988333	-69.1445278	Brey 70a	WN3/WCE	5.05	-9.70	1
84.4187500	-69.1326944	Brey 71	WN6	4.70	-9.65	1
84.4431250	-69.1526667	Brey 73	WN6h	4.65	-8.75	1
84.4484167	-69.3537778	[M2002]LMC 169271	WN3+O7V	-	low	
84.6008750	-69.4870556	LHA 120-S 131	WN11	-	low	
84.6154583	-69.4995833	HD 269908	WN3/4pec	5.15	-9.70	1
84.7420417	-69.4887500	Brey 91	WN9	4.51	-9.15	1
84.9007500	-69.6531111	Brey 93a	WN3	4.80	-8.83	1
85.2116667	-69.4421667	Brey 96	WN3	5.05	-8.80	1
86.1292917	-69.3376389	Sk-69 296	WN11	4.45	-9.40	1
86.2238333	-67.1767222	Brey 98	WN4	4.85	-9.38	1
86.3506667	-67.0991111	Brey 99	WN4	4.90	-9.15	1
86.6931250	-67.1661944	HD 270149	WN3	4.90	-8.98	1
WN3/O3 ( $-9.7 \leq M_{Bol} < -8$ )						
74.2032917	-69.6113056	[MNM2015]LMCe055-1	WN4/O4	4.97	-7.63	8
76.1360000	-68.0165000	[MNM2014]LMC277-2	WN3/O3	5.00	-9.70	7
76.8055417	-70.5594167	[M2002]LMC 71747	WN3/O3	4.98	-9.18	7
80.3450833	-65.8802222	[MNM2015]LMCe169-1	WN3/O3	5.00	-8.28	7
81.2369583	-66.4456667	[MNM2015]LMCe159-1	WN3/O3	5.01	-9.53	7
82.1130000	-69.1100556	[MNM2014]LMC199-1	WN3/O3	5.00	-8.88	7
82.3257917	-69.3286667	[M2002]LMC 143741	WN3/O3	5.00	-9.43	7

Table C1 *continued on next page*

**Table C1** (*continued*)

RAJ2000	DecJ2000	Name	SpType	Log( $T_{eff}$ )	$M_{Bol}$	Source <sup>a</sup>
83.7537500	-69.3556111	[MNM2014]LMC172-1	WN3/O3	5.02	-9.85	7
85.0148750	-69.6314167	[MNM2014]LMC174-1	WN3/O3	5.00	-8.88	7
85.3229167	-69.1156111	[MNM2015]LMCe078-3	WN3/O3	5.00	-8.60	7

<sup>a</sup> Source of  $\log(T_{eff})$  and  $M_{Bol}$ : 1 =Hainich et al. (2014), 2 =Massey et al. (2000), 3 =Bestenlehner et al. (2014), 4 =Testor & Niemela (1998), 5 =Gvaramadze et al. (2014), 6 =Crowther et al. (2023), 7 =Neugent et al. (2017), 8 =Massey et al. (2024)

**Table C3.** Wolf-Rayet Slash Stars in the LMC

RAJ2000	DecJ2000	Name	SpType	Log( $T_{eff}$ ) <sup>a</sup>	$M_{Bol}$ <sup>a</sup>
74.3643333	-67.6508056	Brey 10a	O2If*/WN5	4.70	-9.70
78.5732083	-67.3430833	[MNM2015]LMCe132-1	O3.5If*/WN5	-	
80.7490833	-68.0296111	HD 269445	Ofpe/WN9	4.45	-11.45
83.9258333	-69.1982222	Brey 58	O3.5If*/WN7	4.65	-10.20
84.4639167	-69.1629722	Brey 74a	O3If*	4.65	-9.95
84.6618333	-69.1137500	BAT99 97	O3.5If*/WN7	4.65	-10.95
84.6676167	-69.0999444	Brey 78	O2.5If*/WN6	4.65	-9.95
84.6744792	-69.1039722	Brey 76	O2If*/WN5	4.80	-11.48
84.6754833	-69.0986667	Brey 77	O2If*	4.70	-11.20
84.6767000	-69.1041667	4 R136-015	O2If*/WN5	-	-11.93
84.6767917	-69.1007500	BAT99 110	O2If*/O3If*/WN6	4.70	-10.75
84.6795833	-69.0963333	BAT99 113	O2If*/WN5	4.70	-10.43
84.6800458	-69.1040000	BAT99 114	O2If*/WN5	4.80	-11.30

<sup>a</sup>  $\log(T_{eff})$  and  $M_{Bol}$  from Hainich et al. (2014)

**Table C2.** Wolf-Rayet WC and WO in the LMC

RAJ2000	DecJ2000	Name	SpType	$V_{mag}$	$A_V$ <sup>b</sup>	$M_V$	Log( $T_{eff}$ )	$M_{Bol}$	Source <sup>a</sup>
WC									
74.0120000	-69.4559722	HD 32257	WC4	14.23	0.4	-4.67	4.94	-8.90	9
74.0458333	-66.2925000	HD 32125	WC4	14.33	0.5	-4.67	4.92	-8.90	9
74.1442917	-66.4740000	HD 32228	WC4+OB	10.83	0.1	-7.77	-	-	
74.3504167	-68.3992500	HD 32402	WC4	12.96	0.4	-5.94	4.86	-9.85	9
77.4740417	-68.8812500	Brey 16a	WC4	13.74	1.2	-5.96	-	-	
79.8180833	-69.6555556	Brey 22	WC6+O5-6	12.21	0.2	-6.49	-	-	
80.7919167	-71.3474722	HD 36156	WC4+abs	12.66	0.1	-5.94	-	-	
81.5165000	-67.4991944	HD 36402	WC4+abs	11.62	0.2	-7.08	5.01	-9.53	7
81.6260833	-68.8409722	HD 36521	WC4+O6III/V	12.32	0.1	-6.28	-	-	
82.5506667	-67.4356389	HD 37026	WC4	13.56	0.3	-5.24	4.92	-9.33	9

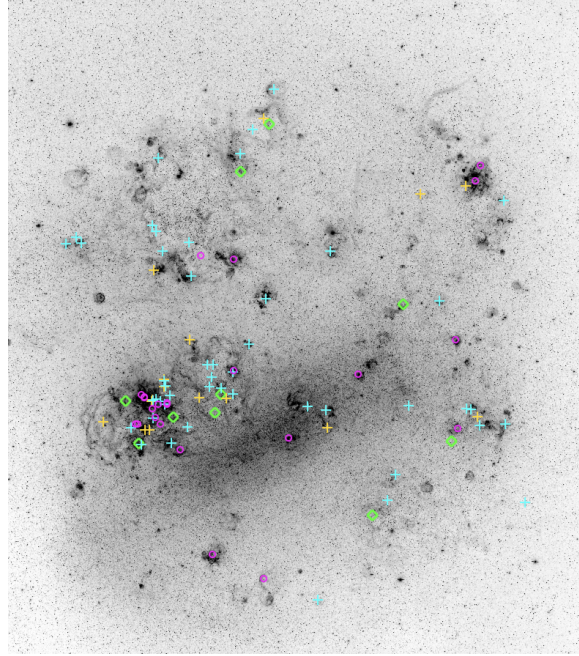
**Table C2** *continued on next page*

Table C2 (*continued*)

RAJ2000	DecJ2000	Name	SpType	$V_{mag}$	$A_V$ <sup>b</sup>	$M_V$	$\text{Log}(T_{eff})$	$M_{Bol}$	Source <sup>a</sup>
82.6612500	-71.0299444	HD 37248	WC4+abs	12.96	0.4	-5.94	-	-	
83.5801667	-69.7528611	HD 37680	WC4	13.12	0.5	-5.88	4.86	-9.90	9
83.9248333	-69.1980278	Brey 58a	WC4	16.52	-	-	-	-	
83.9312083	-69.1827778	Brey 62	WC4	13.96	1.5	-6.04	-	-	
84.2140833	-69.4324167	HD 38030	WC4(+OB)	12.99	0.5	-6.01	-	-	
84.2277500	-69.1939722	Brey 67	WC4(+OB)	12.18	1.1	-7.42	-	-	
84.3718333	-69.3465278	Brey 70	WC4	13.69	-	-	-	-	
84.4360000	-69.2404722	HD 269888	WC4	14.63	1.1	-4.97	4.93	-8.93	9
84.6733333	-69.0872222	RMC140	WC4	12.2	-	-	-	-	
84.6835958	-69.0987500	Brey 83	WC5	14.47	1.6	-5.63	-	-	
84.7657500	-69.0629167	Brey 90a	WC4	15.83	2.2	-4.87	-	-	
84.9837917	-69.4067500	HD 38448	WC4+abs	13	-	-	4.88	-	4
85.0544167	-69.4011667	Brey 95a	WC4+O	13.3	-	-	-	-	
WO									
79.5430417	-69.2173611	[MNM2014]LMC195-1	WO2	15.15	0.40	-3.75	5.05	-8.73	1
79.5453333	-69.2198333	[L72]LH41-1042	WO4	14.00	0.40	-4.9	-	-8.33	4
84.8928750	-68.7358889	Brey 93	WO3	15.20	0.50	-3.8	5.04	-8.73	1

<sup>a</sup> Source of  $\log(T_{eff})$  and  $M_{Bol}$ : 1 =Aadland et al. (2022), 2 =Testor & Niemela (1998), 3 =Neugent et al. (2017), 4 =Crowther et al. (2023)

<sup>b</sup> Derived by Crowther et al. (2023).



**Figure C1.** An H-alpha emission image of the LMC from MCELS (Smith & MCELS Team 1999) with earlier type WN (WN2-WN4, cyan crosses), later type WN (WN5-WN11, yellow crosses), and WN3/O3 (green diamonds) in the luminosity range from  $-9.7 \leq M_{Bol} < -8$ . WC (magenta circles) of all luminosity types are also plotted.

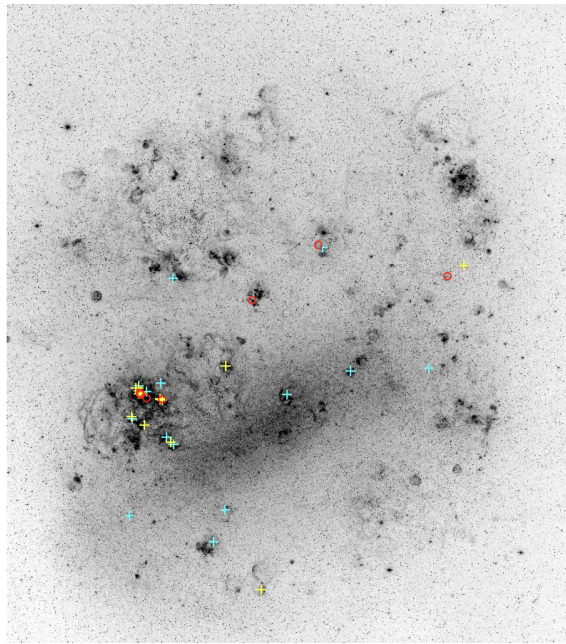


**Figure C2.** An H-alpha emission image of the LMC from MCELS (Smith & MCELS Team 1999) with earlier type WN (WN3-WN4.5, cyan crosses), later type WN (WN5-WN7, yellow crosses), and Of/WN slash stars (red circles) in the highest luminosity range for stars brighter than  $M_{\text{Bol}} < -9.7$

## REFERENCES

- Aadland, E., Massey, P., Hillier, D. J., et al. 2022, ApJ, 931, 157, doi: [10.3847/1538-4357/ac66e7](https://doi.org/10.3847/1538-4357/ac66e7)
- Aadland, E., Massey, P., Neugent, K. F., & Drout, M. R. 2018, AJ, 156, 294, doi: [10.3847/1538-3881/aaeb96](https://doi.org/10.3847/1538-3881/aaeb96)
- Aghakhanloo, M., Smith, N., Andrews, J., et al. 2022, MNRAS, 516, 2142, doi: [10.1093/mnras/stac2265](https://doi.org/10.1093/mnras/stac2265)
- AglioZZo, C., Mehner, A., Phillips, N. M., et al. 2019, A&A, 626, A126, doi: [10.1051/0004-6361/201935239](https://doi.org/10.1051/0004-6361/201935239)
- AglioZZo, C., Phillips, N., Mehner, A., et al. 2021, A&A, 655, A98, doi: [10.1051/0004-6361/202141279](https://doi.org/10.1051/0004-6361/202141279)
- Ardeberg, A., Brunet, J. P., Maurice, E., & Prevot, L. 1972, A&AS, 6, 249
- Aret, A., Kraus, M., Muratore, M. F., & Borges Fernandes, M. 2012, MNRAS, 423, 284, doi: [10.1111/j.1365-2966.2012.20871.x](https://doi.org/10.1111/j.1365-2966.2012.20871.x)
- Asa'd, R. S., Vazdekis, A., & Zeinelabdin, S. 2016, MNRAS, 457, 2151, doi: [10.1093/mnras/stw015](https://doi.org/10.1093/mnras/stw015)
- Bestenlehner, J. M., Crowther, P. A., Broos, P. S., Pollock, A. M. T., & Townsley, L. K. 2022, MNRAS, 510, 6133, doi: [10.1093/mnras/stab3521](https://doi.org/10.1093/mnras/stab3521)
- Bestenlehner, J. M., Gräfener, G., Vink, J. S., et al. 2014, A&A, 570, A38, doi: [10.1051/0004-6361/201423643](https://doi.org/10.1051/0004-6361/201423643)
- Bica, E., Bonatto, C., Dutra, C. M., & Santos, J. F. C. 2008, MNRAS, 389, 678, doi: [10.1111/j.1365-2966.2008.13612.x](https://doi.org/10.1111/j.1365-2966.2008.13612.x)
- Bica, E., Claria, J. J., Dottori, H., Santos, J. F. C., J., & Piatti, A. E. 1996, ApJS, 102, 57, doi: [10.1086/192251](https://doi.org/10.1086/192251)
- Britavskiy, N., Lennon, D. J., Patrick, L. R., et al. 2019, A&A, 624, A128, doi: [10.1051/0004-6361/201834564](https://doi.org/10.1051/0004-6361/201834564)
- Cassatella, A., Barbero, J., Brocato, E., Castellani, V., & Geyer, E. H. 1996, A&A, 306, 125
- Castro, N., Crowther, P. A., Evans, C. J., et al. 2021, A&A, 648, A65, doi: [10.1051/0004-6361/202040008](https://doi.org/10.1051/0004-6361/202040008)
- Cidale, L., Zorec, J., & Tringaniello, L. 2001, A&A, 368, 160, doi: [10.1051/0004-6361:20000409](https://doi.org/10.1051/0004-6361:20000409)
- Condori, C. A. H., Borges Fernandes, M., Kraus, M., Panoglou, D., & Guerrero, C. A. 2019, MNRAS, 488, 1090, doi: [10.1093/mnras/stz1540](https://doi.org/10.1093/mnras/stz1540)

- Conti, P. 1996, in *Liege International Astrophysical Colloquia*, Vol. 33, Liege International Astrophysical Colloquia, ed. J. M. Vreux, A. Detal, D. Fraipont-Caro, E. Gosset, & G. Rauw, 655
- Conti, P. S., Garmany, C. D., De Loore, C., & Vanbeveren, D. 1983, *ApJ*, 274, 302, doi: [10.1086/161447](https://doi.org/10.1086/161447)
- Conti, P. S., Garmany, C. D., & Massey, P. 1986, *AJ*, 92, 48, doi: [10.1086/114133](https://doi.org/10.1086/114133)
- Copetti, M. V. F., Pastoriza, M. G., & Dottori, H. A. 1985, *A&A*, 152, 427
- Crowther, P. A., Rate, G., & Bestenlehner, J. M. 2023, *MNRAS*, 521, 585, doi: [10.1093/mnras/stad418](https://doi.org/10.1093/mnras/stad418)
- Crowther, P. A., & Smith, L. J. 1997, *A&A*, 320, 500
- Crowther, P. A., & Walborn, N. R. 2011, *MNRAS*, 416, 1311, doi: [10.1111/j.1365-2966.2011.19129.x](https://doi.org/10.1111/j.1365-2966.2011.19129.x)
- Cutri, R. M., Skrutskie, M. F., van Dyk, S., et al. 2003, *VizieR Online Data Catalog: 2MASS All-Sky Catalog of Point Sources (Cutri+2003)*, *VizieR On-line Data Catalog: II/246*. Originally published in: 2003yCat.2246....0C
- Davidson, K. 2020, *Galaxies*, 8, 10, doi: [10.3390/galaxies8010010](https://doi.org/10.3390/galaxies8010010)
- Davidson, K., Humphreys, R. M., & Weis, K. 2016, *arXiv e-prints*, arXiv:1608.02007, doi: [10.48550/arXiv.1608.02007](https://doi.org/10.48550/arXiv.1608.02007)
- Davies, B., Crowther, P. A., & Beasor, E. R. 2018, *MNRAS*, 478, 3138, doi: [10.1093/mnras/sty1302](https://doi.org/10.1093/mnras/sty1302)
- Davies, R. D., Elliott, K. H., & Meaburn, J. 1976, *MmRAS*, 81, 89
- de Wit, W. J., Oudmaijer, R. D., van den Ancker, M. E., & Calvet, N. 2014, *The Messenger*, 157, 50
- Deman, J. A., & Oey, M. S. 2024, *ApJ*, 976, 125, doi: [10.3847/1538-4357/ad813410.1134/S1063772908070019](https://doi.org/10.3847/1538-4357/ad813410.1134/S1063772908070019)
- Doran, E. I., Crowther, P. A., de Koter, A., et al. 2013, *A&A*, 558, A134, doi: [10.1051/0004-6361/201321824](https://doi.org/10.1051/0004-6361/201321824)
- Eggenberger, P., Ekström, S., Georgy, C., et al. 2021, *A&A*, 652, A137, doi: [10.1051/0004-6361/202141222](https://doi.org/10.1051/0004-6361/202141222)
- Evans, C. J., Taylor, W. D., Hénault-Brunet, V., et al. 2011, *A&A*, 530, A108, doi: [10.1051/0004-6361/201116782](https://doi.org/10.1051/0004-6361/201116782)
- Evans, C. J., Kennedy, M. B., Dufton, P. L., et al. 2015, *A&A*, 574, A13, doi: [10.1051/0004-6361/201424414](https://doi.org/10.1051/0004-6361/201424414)
- Fariña, C., Bosch, G. L., Morrell, N. I., Barbá, R. H., & Walborn, N. R. 2009, *AJ*, 138, 510, doi: [10.1088/0004-6256/138/2/510](https://doi.org/10.1088/0004-6256/138/2/510)
- Feast, M. W., Thackeray, A. D., & Wesselink, A. J. 1960, *MNRAS*, 121, 337, doi: [10.1093/mnras/121.4.337](https://doi.org/10.1093/mnras/121.4.337)
- Frogel, J. A., & Cohen, J. G. 1982, *ApJ*, 253, 580, doi: [10.1086/159660](https://doi.org/10.1086/159660)
- Gamow, G. 1943, *ApJ*, 98, 500, doi: [10.1086/144581](https://doi.org/10.1086/144581)
- Glatt, K., Grebel, E. K., & Koch, A. 2010, *A&A*, 517, A50, doi: [10.1051/0004-6361/201014187](https://doi.org/10.1051/0004-6361/201014187)
- González-Fernández, C., Dorda, R., Negueruela, I., & Marco, A. 2015, *A&A*, 578, A3, doi: [10.1051/0004-6361/201425362](https://doi.org/10.1051/0004-6361/201425362)
- Gummersbach, C. A., Zickgraf, F. J., & Wolf, B. 1995, *A&A*, 302, 409
- Gvaramadze, V. V., Chené, A. N., Kniazev, A. Y., et al. 2014, *MNRAS*, 442, 929, doi: [10.1093/mnras/stu909](https://doi.org/10.1093/mnras/stu909)
- Hainich, R., Rühling, U., Todt, H., et al. 2014, *A&A*, 565, A27, doi: [10.1051/0004-6361/201322696](https://doi.org/10.1051/0004-6361/201322696)
- Hamann, W. R., Duennebeil, G., Koesterke, L., Wessolowski, U., & Schmutz, W. 1991, *A&A*, 249, 443
- Hénault-Brunet, V., Evans, C. J., Sana, H., et al. 2012, *A&A*, 546, A73, doi: [10.1051/0004-6361/201219471](https://doi.org/10.1051/0004-6361/201219471)
- Heydari-Malayeri, M., Meynadier, F., & Walborn, N. R. 2003, *A&A*, 400, 923, doi: [10.1051/0004-6361:20030066](https://doi.org/10.1051/0004-6361:20030066)
- Hill, R. J., Madore, B. F., & Freedman, W. L. 1994, *ApJS*, 91, 583, doi: [10.1086/191949](https://doi.org/10.1086/191949)
- Hodge, P. W. 1983, *ApJ*, 264, 470, doi: [10.1086/160615](https://doi.org/10.1086/160615)
- Høg, E., Fabricius, C., Makarov, V. V., et al. 2000, *A&A*, 355, L27
- Houk, N., & Cowley, A. P. 1975, *University of Michigan Catalogue of two-dimensional spectral types for the HD stars. Volume I. Declinations -90\_ to -53.f0*.
- Humphreys, R. M. 1979, *ApJS*, 39, 389, doi: [10.1086/190578](https://doi.org/10.1086/190578)
- Humphreys, R. M., & Davidson, K. 1979, *ApJ*, 232, 409, doi: [10.1086/157301](https://doi.org/10.1086/157301)
- . 1994, *PASP*, 106, 1025, doi: [10.1086/133478](https://doi.org/10.1086/133478)



- Humphreys, R. M., Davidson, K., Hahn, D., Martin, J. C., & Weis, K. 2017, *ApJ*, 844, 40, doi: [10.3847/1538-4357/aa7cef](https://doi.org/10.3847/1538-4357/aa7cef)
- Humphreys, R. M., Jones, T. J., & Martin, J. C. 2023, *AJ*, 166, 50, doi: [10.3847/1538-3881/acdd6c](https://doi.org/10.3847/1538-3881/acdd6c)
- Humphreys, R. M., Weis, K., Davidson, K., & Gordon, M. S. 2016, *ApJ*, 825, 64, doi: [10.3847/0004-637X/825/1/64](https://doi.org/10.3847/0004-637X/825/1/64)
- Hung, C. S., Ou, P.-S., Chu, Y.-H., Gruendl, R. A., & Li, C.-J. 2021, *ApJS*, 252, 21, doi: [10.3847/1538-4365/abcc00](https://doi.org/10.3847/1538-4365/abcc00)
- Hunter, D. A., Elmegreen, B. G., Dupuy, T. J., & Mortonson, M. 2003, *AJ*, 126, 1836, doi: [10.1086/378056](https://doi.org/10.1086/378056)
- Jaschek, M. 1978, Catalog of selected spectral types in the MK system
- Kastner, J. H., Buchanan, C., Sahai, R., Forrest, W. J., & Sargent, B. A. 2010, *AJ*, 139, 1993, doi: [10.1088/0004-6256/139/5/1993](https://doi.org/10.1088/0004-6256/139/5/1993)
- Kim, S., Dopita, M. A., Staveley-Smith, L., & Bessell, M. S. 1999, *AJ*, 118, 2797, doi: [10.1086/301116](https://doi.org/10.1086/301116)
- Kraus, M. 2019, *Galaxies*, 7, 83, doi: [10.3390/galaxies7040083](https://doi.org/10.3390/galaxies7040083)
- Kumar, B., Sagar, R., & Melnick, J. 2008, *MNRAS*, 386, 1380, doi: [10.1111/j.1365-2966.2008.12926.x](https://doi.org/10.1111/j.1365-2966.2008.12926.x)
- Lamers, H. J. G. L. M., Maeder, A., Schmutz, W., & Cassinelli, J. P. 1991, *ApJ*, 368, 538, doi: [10.1086/169717](https://doi.org/10.1086/169717)
- Lamers, H. J. G. L. M., Zickgraf, F.-J., de Winter, D., Houziaux, L., & Zorec, J. 1998, *A&A*, 340, 117
- Leitherer, C., Appenzeller, I., Klare, G., et al. 1985, *A&A*, 153, 168
- Lennon, D. J., van der Marel, R. P., Ramos Lerate, M., O'Mullane, W., & Sahlmann, J. 2017, *A&A*, 603, A75, doi: [10.1051/0004-6361/201630076](https://doi.org/10.1051/0004-6361/201630076)
- Liu, Z., Cui, W., Zhao, G., et al. 2023, *MNRAS*, 519, 995, doi: [10.1093/mnras/stac3562](https://doi.org/10.1093/mnras/stac3562)
- Martin, J. C. 2006, *AJ*, 131, 3047, doi: [10.1086/504079](https://doi.org/10.1086/504079)
- Martin, J. C., & Humphreys, R. M. 2023, *AJ*, 166, 214, doi: [10.3847/1538-3881/ad011e](https://doi.org/10.3847/1538-3881/ad011e)
- Massey, P. 2002, *ApJS*, 141, 81, doi: [10.1086/338286](https://doi.org/10.1086/338286)
- Massey, P., Neugent, K. F., & Morrell, N. 2015, *ApJ*, 807, 81, doi: [10.1088/0004-637X/807/1/81](https://doi.org/10.1088/0004-637X/807/1/81)
- . 2017, *ApJ*, 837, 122, doi: [10.3847/1538-4357/aa5d17](https://doi.org/10.3847/1538-4357/aa5d17)
- Massey, P., Neugent, K. F., Morrell, N., & Hillier, D. J. 2014, *ApJ*, 788, 83, doi: [10.1088/0004-637X/788/1/83](https://doi.org/10.1088/0004-637X/788/1/83)
- Massey, P., Neugent, K. F., Morrell, N. I., Hillier, D. J., & Penny, L. R. 2024, *ApJ*, 977, 82, doi: [10.3847/1538-4357/ad8a59](https://doi.org/10.3847/1538-4357/ad8a59)
- Massey, P., Puls, J., Pauldrach, A. W. A., et al. 2005, *ApJ*, 627, 477, doi: [10.1086/430417](https://doi.org/10.1086/430417)
- Massey, P., Waterhouse, E., & DeGioia-Eastwood, K. 2000, *AJ*, 119, 2214, doi: [10.1086/301345](https://doi.org/10.1086/301345)
- McEvoy, C. M., Dufton, P. L., Smoker, J. V., et al. 2017, *ApJ*, 842, 32, doi: [10.3847/1538-4357/aa745a](https://doi.org/10.3847/1538-4357/aa745a)
- McGregor, P. J., & Hyland, A. R. 1981, *ApJ*, 250, 116, doi: [10.1086/159353](https://doi.org/10.1086/159353)
- Mehner, A., Baade, D., Rivinius, T., et al. 2013a, *A&A*, 555, A116, doi: [10.1051/0004-6361/201321323](https://doi.org/10.1051/0004-6361/201321323)
- . 2013b, *A&A*, 555, A116, doi: [10.1051/0004-6361/201321323](https://doi.org/10.1051/0004-6361/201321323)
- Melnick, J. 1985, *A&A*, 153, 235
- Meynet, G., & Maeder, A. 2005, *A&A*, 429, 581, doi: [10.1051/0004-6361:20047106](https://doi.org/10.1051/0004-6361:20047106)
- Moffat, A. F. J. 1991, *A&A*, 244, L9
- Neugent, K. F., Massey, P., Hillier, D. J., & Morrell, N. 2017, *ApJ*, 841, 20, doi: [10.3847/1538-4357/aa6e51](https://doi.org/10.3847/1538-4357/aa6e51)
- Neugent, K. F., Massey, P., & Morrell, N. 2018, *ApJ*, 863, 181, doi: [10.3847/1538-4357/aad17d](https://doi.org/10.3847/1538-4357/aad17d)
- Oey, M. S. 1996, *ApJ*, 465, 231, doi: [10.1086/177415](https://doi.org/10.1086/177415)
- Oksala, M. E., Kraus, M., Cidale, L. S., Muratore, M. F., & Borges Fernandes, M. 2013, *A&A*, 558, A17, doi: [10.1051/0004-6361/201321568](https://doi.org/10.1051/0004-6361/201321568)
- Parker, J. W. 1993, *AJ*, 106, 560, doi: [10.1086/116661](https://doi.org/10.1086/116661)
- Parker, J. W., Clayton, G. C., Winge, C., & Conti, P. S. 1993, *ApJ*, 409, 770, doi: [10.1086/172706](https://doi.org/10.1086/172706)
- Parker, J. W., & Garmany, C. D. 1993, *AJ*, 106, 1471, doi: [10.1086/116740](https://doi.org/10.1086/116740)
- Phillips, G. D., Oey, M. S., Cuevas, M., Castro, N., & Kothari, R. 2024, *ApJ*, 966, 243, doi: [10.3847/1538-4357/ad3909](https://doi.org/10.3847/1538-4357/ad3909)
- Popescu, B., Hanson, M. M., & Elmegreen, B. G. 2012, *ApJ*, 751, 122, doi: [10.1088/0004-637X/751/2/122](https://doi.org/10.1088/0004-637X/751/2/122)



- Press, W. H., Flannery, B. P., & Teukolsky, S. A. 1986, *Numerical recipes. The art of scientific computing*
- Reid, W. A., & Parker, Q. A. 2012, *MNRAS*, 425, 355, doi: [10.1111/j.1365-2966.2012.21471.x](https://doi.org/10.1111/j.1365-2966.2012.21471.x)
- Richardson, N. D., & Mehner, A. 2018, *Research Notes of the American Astronomical Society*, 2, 121, doi: [10.3847/2515-5172/aad1f3](https://doi.org/10.3847/2515-5172/aad1f3)
- Rousseau, J., Martin, N., Prévot, L., et al. 1978, *A&AS*, 31, 243
- Sabín-Sanjulián, C., Simón-Díaz, S., Herrero, A., et al. 2017, *A&A*, 601, A79, doi: [10.1051/0004-6361/201629210](https://doi.org/10.1051/0004-6361/201629210)
- Sanduleak, N. 1970, *Contributions from the Cerro Tololo Inter-American Observatory*, 89
- Shore, S. N., & Sanduleak, N. 1983, *ApJ*, 273, 177, doi: [10.1086/161356](https://doi.org/10.1086/161356)
- . 1984, *ApJS*, 55, 1, doi: [10.1086/190945](https://doi.org/10.1086/190945)
- Smith, L. F., Shara, M. M., & Moffat, A. F. J. 1990, *ApJ*, 348, 471, doi: [10.1086/168256](https://doi.org/10.1086/168256)
- Smith, N. 2019, *MNRAS*, 489, 4378, doi: [10.1093/mnras/stz2277](https://doi.org/10.1093/mnras/stz2277)
- Smith, N., & Tombleson, R. 2015, *MNRAS*, 447, 598, doi: [10.1093/mnras/stu2430](https://doi.org/10.1093/mnras/stu2430)
- Smith, R. C., & MCELS Team. 1999, in *IAU Symposium*, Vol. 190, *New Views of the Magellanic Clouds*, ed. Y. H. Chu, N. Suntzeff, J. Hesser, & D. Bohlender, 28
- Stahl, O., & Wolf, B. 1986, *A&A*, 154, 243
- Stahl, O., Wolf, B., Klare, G., et al. 1983, *A&A*, 127, 49
- Stahl, O., Wolf, B., Klare, G., Juettner, A., & Cassatella, A. 1990, *A&A*, 228, 379
- Stahl, O., Wolf, B., & Zickgraf, F. J. 1987, *A&A*, 184, 193
- Tarrab, I. 1985, *A&A*, 150, 151
- Testor, G., & Niemela, V. 1998, *A&AS*, 130, 527, doi: [10.1051/aas:1998241](https://doi.org/10.1051/aas:1998241)
- Torres, A. F., Cidale, L. S., Kraus, M., et al. 2018, *A&A*, 612, A113, doi: [10.1051/0004-6361/201731723](https://doi.org/10.1051/0004-6361/201731723)
- Tubbesing, S., Kaufer, A., Stahl, O., et al. 2002, *A&A*, 389, 931, doi: [10.1051/0004-6361:20020682](https://doi.org/10.1051/0004-6361:20020682)
- Udalski, A., Szymanski, M., Kubiak, M., et al. 2000, *AcA*, 50, 307, doi: [10.48550/arXiv.astro-ph/0010150](https://doi.org/10.48550/arXiv.astro-ph/0010150)
- van Genderen, A. M. 2001, *A&A*, 366, 508, doi: [10.1051/0004-6361:20000022](https://doi.org/10.1051/0004-6361:20000022)
- van Genderen, A. M., & Sterken, C. 1996, *A&A*, 308, 763
- . 1999, *A&A*, 349, 537
- van Loon, J. T., Marshall, J. R., & Zijlstra, A. A. 2005, *A&A*, 442, 597, doi: [10.1051/0004-6361:20053528](https://doi.org/10.1051/0004-6361:20053528)
- Walborn, N. R., & Blades, J. C. 1997, *ApJS*, 112, 457, doi: [10.1086/313043](https://doi.org/10.1086/313043)
- Walborn, N. R., Drissen, L., Parker, J. W., et al. 1999, *AJ*, 118, 1684, doi: [10.1086/301038](https://doi.org/10.1086/301038)
- Walborn, N. R., Gamen, R. C., Morrell, N. I., et al. 2017, *AJ*, 154, 15, doi: [10.3847/1538-3881/aa6195](https://doi.org/10.3847/1538-3881/aa6195)
- Walborn, N. R., Howarth, I. D., Evans, C. J., et al. 2010, *AJ*, 139, 1283, doi: [10.1088/0004-6256/139/3/1283](https://doi.org/10.1088/0004-6256/139/3/1283)
- Walborn, N. R., Sana, H., Simón-Díaz, S., et al. 2014a, *A&A*, 564, A40, doi: [10.1051/0004-6361/201323082](https://doi.org/10.1051/0004-6361/201323082)
- . 2014b, *A&A*, 564, A40, doi: [10.1051/0004-6361/201323082](https://doi.org/10.1051/0004-6361/201323082)
- Wenger, M., Ochsenbein, F., Egret, D., et al. 2000, *A&AS*, 143, 9, doi: [10.1051/aas:2000332](https://doi.org/10.1051/aas:2000332)
- Wolf, B., Stahl, O., de Groot, M. J. H., & Sterken, C. 1981, *A&A*, 99, 351
- Wolf, M. J., Drory, N., Gebhardt, K., & Hill, G. J. 2007, *ApJ*, 655, 179, doi: [10.1086/509768](https://doi.org/10.1086/509768)
- Zaritsky, D., Harris, J., Thompson, I. B., & Grebel, E. K. 2004, *AJ*, 128, 1606, doi: [10.1086/423910](https://doi.org/10.1086/423910)
- Zickgraf, F. J., Wolf, B., Stahl, O., & Humphreys, R. M. 1989, *A&A*, 220, 206
- Zickgraf, F. J., Wolf, B., Stahl, O., Leitherer, C., & Appenzeller, I. 1986, *A&A*, 163, 119